

This is a non peer reviewed preprint submitted to EarthArxiv, with planned submission to Volcanica after some feedback based on this preprint!

DiadFit: An Open-SourcePython3 Tool for Peak fitting of Raman Data from silicate melts and CO<sub>2</sub> fluids

Penny E. Wieser<sup>1</sup> and Charlotte DeVitre<sup>1</sup>

Earth and Planetary Sciences, UC Berkeley

This tool is for you – the Raman and CO<sub>2</sub>- loving community. We have posted this preprint to give you a chance to try the code. Doesn't work for your instrument or your file type? Please send me some examples, and I will tweak it so it does!

[Penny\\_wieser@berkeley.edu](mailto:Penny_wieser@berkeley.edu), or raise an issue on GitHub - <https://github.com/PennyWieser/DiadFit>

---

# DIADFIT: AN OPEN-SOURCE PYTHON3 TOOL FOR PEAK FITTING OF RAMAN DATA FROM SILICATE MELTS AND CO<sub>2</sub> FLUIDS

Penny E. Wieser<sup>‡</sup>, Charlotte L. DeVitre<sup>‡</sup>

## ABSTRACT

We present DiadFit - an open-source Python3 tool for efficient processing of Raman spectroscopy data collected from silicate melts and CO<sub>2</sub> fluids. DiadFit can fit Fermi diads, hot bands, <sup>13</sup>C peaks, peaks from other gas species (e.g. SO<sub>2</sub>, N<sub>2</sub>), and Ne lines using various background and peak shapes. Thus, it is highly suited for workflows involving melt inclusion vapour bubbles and fluid inclusions (FI). It can also convert between temperature, pressure and density using the CO<sub>2</sub> equation of state (EOS), allowing calculation of FI entrapment pressures (and depths in the crust), conversion of  $T_{homog}$  from microthermometry measurements to CO<sub>2</sub> density, and propagation of uncertainties associated with EOS calculations using Monte Carlo methods. There are also functions to quantify the area ratio of the silicate vs. H<sub>2</sub>O region of spectra collected on silicate glasses to determine H<sub>2</sub>O contents. Documentation and worked examples are available (<https://bit.ly/DiadFitRTD>, <https://bit.ly/DiadFitYouTube>).

## 1 INTRODUCTION

In recent years, Raman Spectroscopy has been increasingly used by igneous petrologists to perform non-destructive, in-situ measurements of melt and fluid compositions (Steele-Macinnis et al. [2011], Hartley et al. [2014], Moore et al. [2015], González-García et al. [2020], Giordano et al. [2020], Schiavi et al. [2020], Morizet et al. [2013], Schiavi et al. [2018]). Since 2014, there has been a growing body of literature using Raman Spectroscopy to measure the density of CO<sub>2</sub>-rich fluids in melt inclusion vapour bubbles to more accurately obtain the total CO<sub>2</sub> content of the melt inclusion, and thus the magma storage depth (Hartley et al. [2014], Moore et al. [2015], Wieser et al. [2021], Lamadrid et al. [2017], Allison et al. [2021], DeVitre et al. [2023b]). Raman spectroscopy also shows enormous potential to quantify the densities of CO<sub>2</sub>-rich fluid inclusions (Wang et al. [2011], Kobayashi et al. [2012]), allowing rapid and precise estimates of magma storage depths (Dayton et al. [2023]).

However, while there have been a large number of studies optimizing calibration and analysis protocols for CO<sub>2</sub>-rich fluids by Raman Spectroscopy (e.g., Lamadrid et al. [2017], DeVitre et al. [2021], Bakker [2021]), there has been comparatively less focus on the software tools and peak fitting rou-

tines used to fit Raman spectral data (e.g. Yuan and Mayanovic [2017]). Many studies use proprietary software supplied as part of the Raman spectrometer for peak fitting (e.g. Moore et al. [2015]), which affects reproducibility because data is collected (and thus processed) on different Raman instruments (e.g., WITec, HORIBA, Bruker, Renishaw). One popular open-source option is a GUI-based peak fitting program called Fityk (Wojdyr [2010]). While scripting is possible in this tool, most users fit curves by manually clicking to select peak and background positions (e.g. DeVitre et al. [2021]). Other studies use OriginLab software which has an annual subscription fee of ~ 200 USD per license per year (e.g., Hartley et al. [2014]), or have developed their own Matlab/Python codes for specific workflows and instruments (e.g., Wieser et al. [2021], Allison et al. [2021]). We do not believe any of the existing data processing methods have been fully optimized for the specific Raman spectroscopy workflows becoming widespread in volcanology. There are also no widely-available scripting tools for common calculations associated with fluid inclusion data, such as calculating CO<sub>2</sub> densities from microthermometry data, and converting CO<sub>2</sub> densities from fluid inclusions into pressure and depths using the CO<sub>2</sub> equation of state.

The aim of DiadFit is to provide an open-source, reproducible, easy-to-use, and efficient tool for volcanologists with a wide range of coding experience (Fig. 1). The shapes and locations of the Fermi diad

---

\*University of California, Berkeley

†Corresponding author: penny\_wieser@berkeley.edu

‡University of California, Berkeley

and Ne lines are well defined, and spectra collected on any given Raman instrument have similar features. This means there is enormous potential for automation. In addition to reducing time spent data processing, this will also result in more consistent fitting between different groups, increasing reproducibility. DiadFit is designed so that generic peak fit parameters are tweaked for a specific analytical set up. Using these tweaked parameters, hundreds of spectra can be fitted automatically within minutes, eliminating tedious (and subjective) workflows requiring lots of clicking. Additionally, to align with FAIR principles (Findable, Accessible, inter operable, reproducible), users could publish a supporting folder containing their spectra, relevant metadata, and Jupyter notebooks showing exactly how spectra were fitted (e.g. [Dayton et al. \[2023\]](#)).

To demonstrate the time-saving nature of DiadFit, we assess the time taken to fit Neon lines and CO<sub>2</sub> acquisitions collected over a 24 hour period during instrument calibration by [DeVitre et al. \[2021\]](#). Fitting these spectra took ~ 8 hrs to process using Fityk, and ~15 minutes using DiadFit on a typical laptop with 16 GB of RAM. Given the potential for Raman spectroscopy to provide rapid estimates of magma storage depths from fluid inclusions during volcanic crises ([Dayton et al. \[2023\]](#)), it is vital to speed up data processing as much as possible to reap the full benefits of this speedy technique. We anticipate that users who are not familiar with Python will simply use the provided Jupyter Notebooks and narrated YouTube videos, changing simple parameters like the path to their files and peak fit parameters to adjust for the intensity range on their instrument. More experienced coders can use the base functions in DiadFit to create highly customizable workflows to address a number of additional science questions to those targeted here (and build their own functions).

## 2 INSTALLATION

DiadFit can be installed locally on Python versions >=3.7 using either the command prompt (Windows) or the terminal (Mac):

```
pip install DiadFit
```

For Python beginners, we recommend using Jupyter environments (e.g., Jupyter Lab and Jupyter Notebook). In these environments, DiadFit can be installed in a code cell directly:

```
!pip install DiadFit
```

After installation, the user must load DiadFit into their script. Here we load it as `pf`. but users could choose any letters they wish:

```
import DiadFit as pf
```

Any function from DiadFit is then called by typing the chosen abbreviation, followed by a dot, followed by the function name:

```
pf.function_name()
```

Information on what the function does and the required inputs can be accessed using the help function:

```
help(pf.fit_generic_peak)
```

## 3 UNDERLYING DEPENDENCIES

DiadFit uses peak-fitting functions from the Python package `lmfit` ([Newville et al. \[2016\]](#)), which supports iterative fitting of different peak types (e.g., Gaussian, Voigt, Pseudovoigt). The SciPy ([Virtanen et al. \[2020\]](#)) `find_peaks` function is used to identify approximate peaks positions and attributes such as height, prominence, and presence/absence of certain peaks. These estimated peak parameters can be used to subdivide spectra into groups with similar characteristics prior to fitting with `lmfit`. Grouping spectra by characteristics, as well as having good estimates of peak position and prominence, greatly increases computational efficiency during iterative fitting of multiple peaks. Numpy ([Harris et al. \[2020\]](#)) is used for all basic math and regression operations, including fitting splines to spectra, and splitting spectra into particular subregions. Pandas ([pandas development team \[2020\]](#)) is used for importing data from spreadsheet-type datafiles (.xlsx, .csv), and to output fit parameters in a tabular format. Matplotlib ([Hunter \[2007\]](#)) is used for all plots produced by functions. EOS calculations using the [Span and Wagner \[1996\]](#) model are implemented through CoolProp. This package is not a dependency for all of DiadFit, but if users want to perform calculations using this model, they need to have CoolProp installed (or they will receive an error containing installation instructions). Calculations using this EOS should cite both DiadFit and CoolProp.

## 4 SUPPORTED FILE TYPES

DiadFit currently supports data input from the following file types. The name given between quotes is the string that should be entered as the `filetype` argument when loading data:

1. `'headless_txt'`: txt file with no header, with wavenumber in the 1st column and intensity in the 2nd column.

# DiadFit

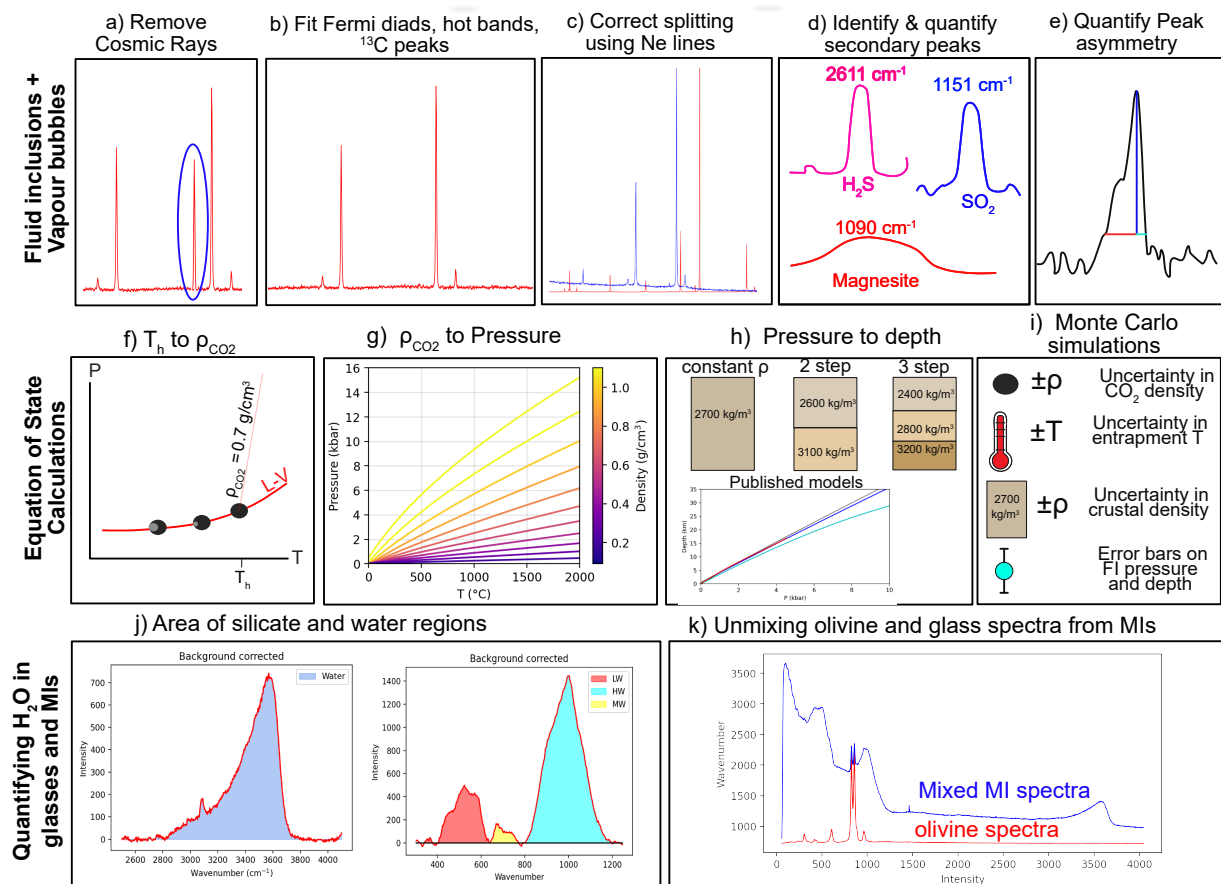


Figure 1: Schematic diagram showing the different workflows that can be performed in DiadFit.

2. `'headless_csv'`: csv file with no header, with wavenumber in the 1st column and intensity in the 2nd column.
3. `'head_csv'`: csv file with a header, with wavenumber in the 1st column and intensity in the 2nd column.
4. `'Witec_ASCII'`: Standard output from WITec Raman instruments. File starts with '//Exported ASCII-File', then has several lines of metadata, before data is listed under a [Data] heading
5. `'HORIBA_txt'`: Standard output on newer HORIBA Raman instruments. It has some metadata rows (e.g., #Acq. time), then data is listed under #Acquired
6. `'Renishaw_txt'`: Standard txt file from a Renishaw instrument, first header is #Wave, second is #Intensity

If your Raman spectrometer outputs a different filetype, please raise an issue on the DiadFit GitHub providing an example file, or contact the author team by email.

## 5 PYTHON JARGON

Different calculations in DiadFit are stored within functions. Each of these functions requires users to enter specific input parameters (called arguments), and the function returns various outputs. Five main datatypes are used in DiadFit as inputs or outputs:

1. A `"string"` is a piece of text. These are used to tell a function something about your data input, or specify a certain thing you want the function to do. For example, users must specify their filetype when using functions that load in spectra (e.g., `filetype='headless_txt'`, see Section 4).
2. A `numpy.array` is a column of data without a heading. DiadFit uses these to store spectral data after it has been extracted from proprietary instrument files. The wavenumber is stored in the 1st column (index 0 in Python), and the intensity in the 2nd column (index 1 in Python). Numpy is used rather than pandas because it allows for very fast computation.
3. A `pandas.Series` is a column of data with a heading.
4. A `pandas.DataFrame` is a collection of `pandas.Series`, and can be visualized as a single sheet in an excel workbook with labelled columns. In DiadFit, these are used to store

peak fitting parameters in columns with column headings (see Step 2, Fig. 5). Information in a given column of the dataframe (called `df`) can be accessed using the column heading: `df['column_heading']`.

5. `dataclasses` are used to provide default configurations to peak finding and fitting functions. These default configurations can be tweaked as much or as little as required for each specific Raman spectrometer. For example, the default parameters for fitting diad 1 are stored in the `dataclass` `diad1_fit_config`:

```
diad1_fit_config(model_name='PseudoVoigtModel',
fit_peaks=2, fit_gauss=False,
gauss_amp=1000, diad_sigma=0.2,
diad_sigma_min_allowance=0.2,
diad_sigma_max_allowance=5,
N_poly_bck_diad1=1,
lower_bck_diad1=(1180, 1220),
upper_bck_diad1=(1300, 1350),
diad_prom=100, HB_prom=20,
x_range_baseline=75, y_range_baseline=100,
plot_figure=True, dpi=200,
x_range_residual=20)
```

Briefly, `model_name='PseudoVoigtModel'` specifies that the diad and hotband peaks should be fitted with a PseudoVoigt function, which is a weighted sum of a Gaussian and Lorentzian distribution that share values for amplitude, center, and full width half maximum. A Voigt distribution function can be used instead simply by stating:

```
pf.diad1_fit_config(model='VoigtModel')
```

Any number of these parameters can be tweaked in this manner. For example, if the user only wants 1 peak (e.g., for weak spectra), wants to fit a third degree polynomial to the background, and wants saved figures showing spectra fits to have a dpi of 300:

```
diad1_fit_config(model='VoigtModel',
fit_peaks=1, N_poly_bck_diad1=3, dpi=300)
```

The idea is once these `dataclasses` are tweaked for a given instrument/set of samples, they can be used to automatically loop through large numbers of spectral files.

## 6 WORKED EXAMPLES

We have produced a number of example Jupyter Notebooks demonstrating specific workflows. These notebooks are available on GitHub and the ReadTheDocs page. We include notebooks showing how to:

1. Fit peaks resulting from CO<sub>2</sub> fluids and correct data for instrument drift using Ne line acquisitions. This example is based on data collected from a high pressure optical cell during Raman densimeter calibration (see [DeVitre et al. \[2021\]](#)).
2. As above, but also showing how to quantify the area of carbonate and SO<sub>2</sub> peaks in spectra collected from natural fluid inclusions hosted in olivine crystals.
3. Fit CO<sub>2</sub> diads and apply a Ne correction model from spectra collected from melt inclusions vapour bubbles using a HORIBA Raman instrument (data from [Wieser et al. \[2021\]](#)).
4. Perform calculations using the CO<sub>2</sub> equation of state, including converting homogenization temperatures from microthermometry into CO<sub>2</sub> densities, converting CO<sub>2</sub> densities from Raman or microthermometry into pressures, and then converting these pressures to depths using different crustal density profiles.
5. Propagate uncertainty in microthermometry and Raman-based fluid inclusion barometry into pressure and depth distributions.
6. Quantify peak asymmetry using the approach of [DeVitre et al. \[2023a\]](#). This can be very helpful to identify fluid inclusions which contain both liquid and vapour phases at the time of analysis.
7. Quantify H<sub>2</sub>O contents in silicate glasses using an approach adapted from [Di Genova et al. \[2017\]](#) and [Schiavi et al. \[2018\]](#).
8. Quantify the ratio of H<sub>2</sub>O to silicate glass peaks on Raman acquisitions taken on unexposed olivine-hosted melt inclusions. This can also be used to quantify H<sub>2</sub>O contents in exposed silicate glasses (following [Di Genova et al. \[2017\]](#)).
9. Propagating Raman and volume uncertainty when determining the contribution from vapour bubble CO<sub>2</sub> to the total CO<sub>2</sub> budget of melt inclusions.

## 7 FITTING THE CO<sub>2</sub> FERMI DIAD

The Raman spectrum of CO<sub>2</sub> consists of two relatively strong, well-defined peaks collectively called the Fermi Diad. These peaks result from the interaction of a symmetrical stretching mode and an active bending mode in the CO<sub>2</sub> molecule by a process known as Fermi resonance ([Lamadrid et al. \[2017\]](#), [Rosso and Bodnar \[1995\]](#), [Fermi \[1931\]](#)). One of

the peaks has a wavenumber of ~1280–1290 cm<sup>-1</sup> (referred to as diad 1), and the second peak has a wavenumber of ~1386–1390 cm<sup>-1</sup> (diad 2, [Fig. 6a](#)). It is well accepted that the distance between diad 1 and diad 2 (commonly referred to as splitting, diad splitting, Fermi Diad separation, or  $\Delta$ ) correlates with the density of the CO<sub>2</sub> fluid. This is because with increasing CO<sub>2</sub> density, diad 1 moves to lower wavenumbers (shift of 6 cm<sup>-1</sup> from 0 to 0.8 g/cm<sup>3</sup>), while the position of diad 2 only varies by ~1–2 cm<sup>-1</sup>. The exact relationship between diad splitting and CO<sub>2</sub> density, commonly called a 'densimeter', has been shown to vary as a function of instrument hardware and acquisition conditions ([DeVitre et al. \[2021\]](#), [Lamadrid et al. \[2017\]](#)).

The Fermi diad is flanked by low intensity hot bands (HBs), which arise from molecules populating the first excited vibron due to their thermal energy at room temperature, which are also perturbed by a Fermi resonance effect. The peak height of the HBs relative to the diads increases with increasing temperature ([Rosso and Bodnar \[1995\]](#)), and in general, hotbands become more pronounced in spectra collected on denser CO<sub>2</sub> fluids. Diad 2 also has a flanking <sup>13</sup>C peak to its left which becomes more visible as the CO<sub>2</sub> density increases and with increasing proportions of <sup>13</sup>C relative to <sup>12</sup>C ([Wang and Lu \[2022\]](#)).

In the literature, density estimates from CO<sub>2</sub>-rich fluids such as melt inclusion vapour bubbles or fluid inclusions have been obtained by fitting the position of the Fermi diad using various background models combined with Voigt, Pseudovoigt, Gaussian or Lorentzian peaks. These peak fitting routines greatly increases the precision at which the diad splitting can be determined relative to the spectral resolution of the instrument (distance between datapoints). While Raman instruments typically acquire an intensity reading every 0.1–1.5 cm<sup>-1</sup>, the error of the peak position on a fitted peak can be 10–30× smaller if an appropriate peak profile is fitted (e.g., voigt/pseudovoigt for diads, [Yuan and Mayanovic \[2017\]](#), [Fukura et al. \[2006\]](#); [Lin et al. \[2007\]](#)). After the peaks are fit, the splitting is calculated and corrected for instrument drift, and then an instrument-specific densimeter should be used to convert splitting into CO<sub>2</sub> density ([Lamadrid et al. \[2017\]](#), [DeVitre et al. \[2021\]](#)).

When using DiadFit to peak fit CO<sub>2</sub> spectra, Step 1 is to find all the spectral files you wish to fit ([Fig. 3](#)). In step 2-5, spectra are divided into groups, because diads can vary greatly in terms of spectral characteristics, and thus the peak fitting routine that should be applied. Spectra collected on CO<sub>2</sub> fluids with low densities, at relatively deep depths, or using low laser power tend to have a weak to non-existent hot bands. Stronger spectra have prominent hot bands and <sup>13</sup>C peaks



which overlap with the tail of the diad peak. In the strongest spectra, the entire region around the diads and hotbands is elevated above the near-linear background seen at greater distance from the diads (Fig. 2). To ensure good fits for all these different spectra types, we suggest users subdivide their spectra into 'Weak', 'Medium' and 'Strong' groups using the steps described below. In Step 2, a single file is selected, and the `identify_diad_peaks` function uses SciPy `find_peaks` to determine approximate peak positions and prominences for the diad, hotbands and <sup>13</sup>C peaks for each spectra. This function also calculates various additional parameters that can help group spectra (e.g. signal to noise ratios, elevation of the diad-HB region above background). The SciPy `find_peaks` parameters will need tweaking based on instrument hardware and acquisition parameters to ensure the function finds all peaks which are visible, and doesn't identify noise as peaks (identified peaks are marked with yellow stars in Step 2). After tweaking these SciPy parameters, all spectra files are looped over in Step 3 to determine the approximate peak parameters for each spectra, and these are saved in a dataframe. In Step 4, these peak parameters are used alongside a filter to remove any cosmic rays present in the spectra. The filtering process calculates the intensity factor  $F$  based on the intensity ( $I$ ) of any given spectral datapoint relative to the intensities of the datapoints to the left and right:

$$F_{i-1} = \frac{I_i - I_{i-1}}{I_{i-1}} \quad (1)$$

$$F_{i+1} = \frac{I_i - I_{i+1}}{I_{i+1}} \quad (2)$$

These two factors are then multiplied together:

$$M_i = F_{i-1} * F_{i+1} \quad (3)$$

If the spectra has a lower intensity to the left of datapoint  $i$ ,  $F_{i-1}$  will be  $>1$ . If the spectra also has lower intensity on the right hand side of point  $i$ ,  $F_{i+1}$  will be  $>1$ , so  $M_i$  will be  $>>1$ . High values of  $M_i$  for individual pixels are indicative of short, sharp peaks (i.e. most cosmic rays). A datapoint is considered a cosmic ray if  $M_i$  exceeds a user determined value (`dynfact`). The highest pixel of Diads, HB and <sup>13</sup>C peaks can also have high  $M_i$  values, so any points with an  $x$  coordinate equal to an identified peak position ( $\pm$  the spectral resolution) are ignored. Users can also enter a custom range, within which no cosmic rays are removed (e.g. the area around the narrow SO<sub>2</sub> peak). If a cosmic ray is identified, the filter is run again, in case the cosmic ray was wider than a single pixel. The pixels identified as cosmic rays are then removed from the spectrum and a new file is saved with the same filename with the addition of the suffix `_CRR_DiadFit`.

After removal of cosmic rays, the `identify_diad_peaks` function is used again to obtain approximate peak parameters without inference from cosmic rays.

In Step 5, the approximate peak parameters from `identify_diad_peaks` are used to divide spectra into groups. A full description of the different parameters used for classification is provided on the ReadTheDocs page, and the most useful parameters will depend greatly on your Raman instrument and samples. In general, spectra should be classified as 'Weak' when none of the peaks are strong enough to interfere with each other (e.g., Fig. 2c). In a set of acquisitions where lots of spectra have no hot band, it would make sense to have the weak group be spectra with only a diad, and no HB. These are best fitted with a single peak (`fit_peaks=1`). If there was then a second group of slightly stronger spectra with a relatively prominent hot band, these could be classified as 'Medium', with 2 peaks fitted around diad 1, and 3 peaks around diad 2. Fitting more peaks helps improve the overall residual because the tails of the diad and hotband peak overlap slightly for higher CO<sub>2</sub> densities, so should be fitted iteratively (Fig. 2f). Spectra with very strong hot bands, clear <sup>13</sup>C peaks, and greatly elevated troughs between diads and HBs should be placed into the 'Strong' category. These spectra will need to be fitted with two/three peaks, and an additional Gaussian background to recreate the elevation of the spectra in the diad region (`fit_gauss=True`).

In the gas-cell calibration data of DeVitre et al. [2021] shown in Fig. 3, all spectra had a visible hotband. Thus, we use the 'Weak' category for spectra with no <sup>13</sup>C peak, and no overlap of the tails of HB2 and Diad2 (Fig. 2c). The remaining spectra could be split in two ways. One option is to classify them all as strong (requiring 3 peaks, and a Gaussian background). If a Gaussian background isn't really required (e.g., Fig. 2f), the code will converge on a Gaussian with a very small amplitude, so the only real advantage of putting those not really needing Gaussian backgrounds into a 'Medium' Category is that the iterative fitting routine will be a bit faster, so it is worth the extra category if you have a lot of spectra to fit.

One file from each group is then used to tweak the fit parameters (Step 6, Fig. 3), which are applied to all spectra in the group (taking 1-5 s per spectra on a 16 GB laptop). A figure of each fit is produced, and should be visually inspected (Step 8). In Step 9, fit parameters determined through looping over each group are merged together, and combined with relevant metadata (e.g. the time stamp needed to apply the Ne correction model). In Step 10, splittings corrected for instrument drift are converted into CO<sub>2</sub> densities using a instrument-specific densimeter. DiadFit incorporates a number of functions

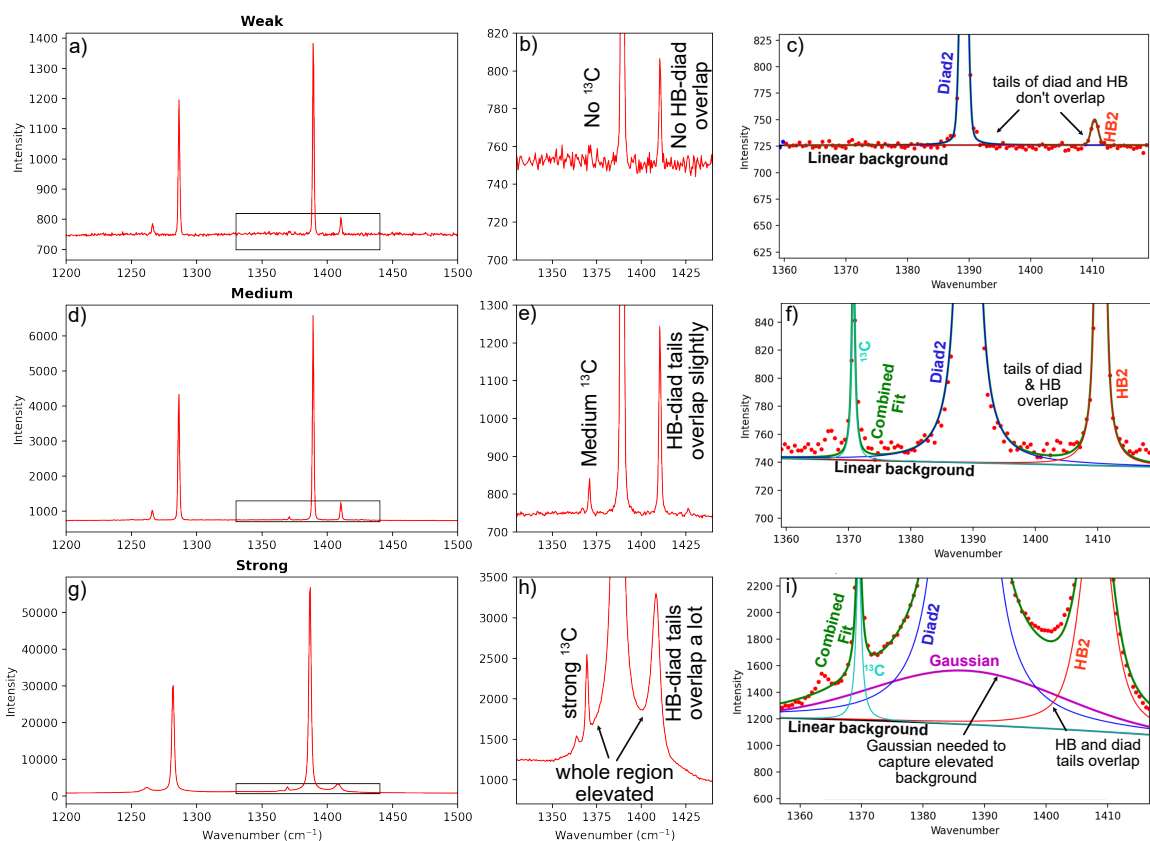


Figure 2: Spectra from DeVitre et al. [2021] with different characteristics can be subdivided into groups for ease of fitting. The weakest spectra (a-c) have no  $^{13}\text{C}$  peak, and a small HB, which does not overlap with the diad (c). These could be fitted with 1 or 2 peaks, because the fitting of the HB doesn't influence the fitting of the diad. Slightly stronger spectra (d-f) have a  $^{13}\text{C}$  peak, and the tails of the  $^{13}\text{C}$ , diad and HB peak all overlap (f). The overlapping tails of these peaks means that 3 peaks need to be fitted iteratively. In the strongest spectra (g-i), the troughs between  $^{13}\text{C}$  and the diad and the diad and the HB are greatly elevated above the background. This requires a Gaussian background in addition to the 3 other peaks to minimise residuals.



to propagate uncertainties (see Section 11.1).

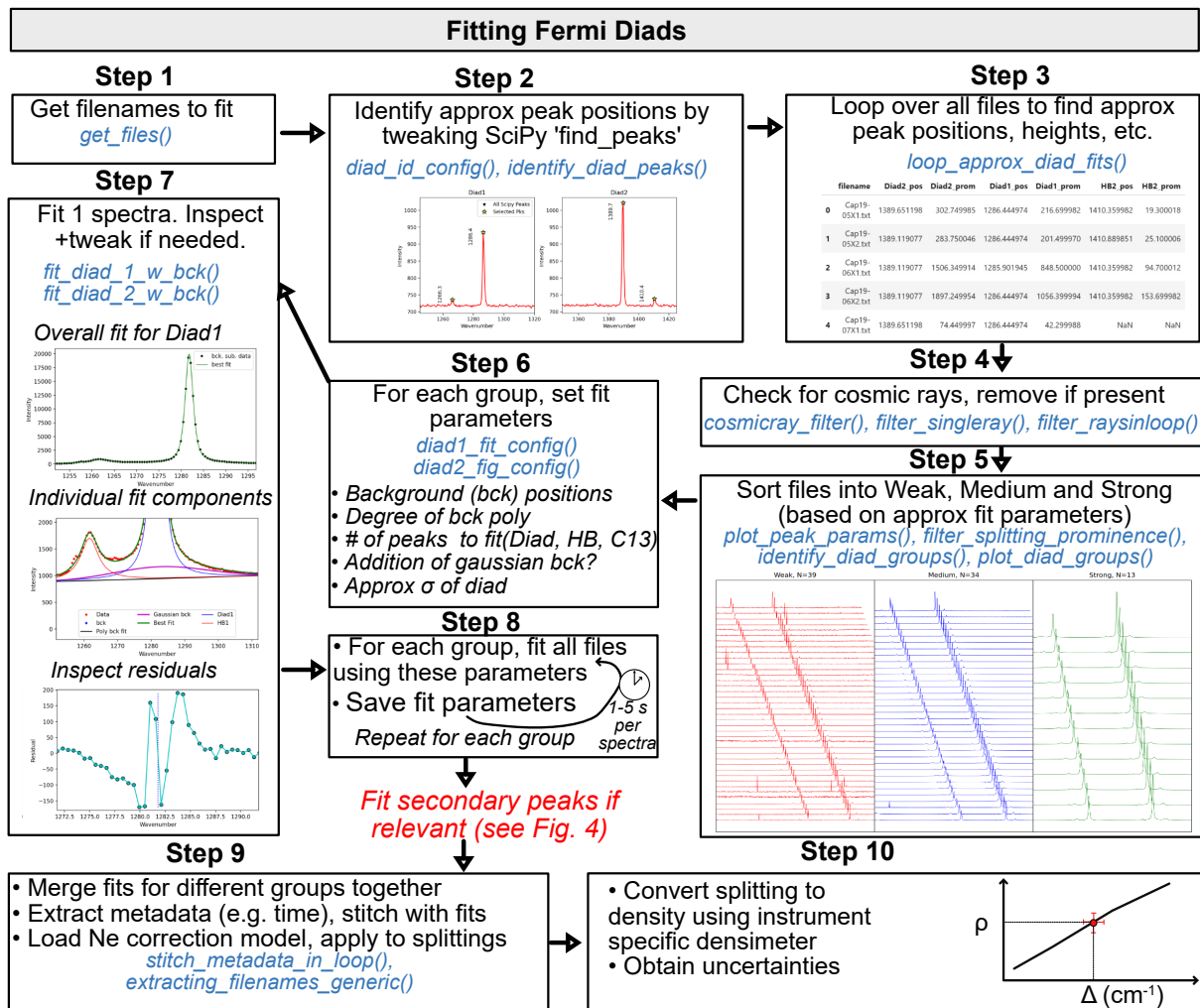


Figure 3: Schematic of workflow used to efficiently fit diad peaks with very different spectral characteristics.

## 7.1 Fitting peaks to secondary phases

Raman spectra collected from fluid inclusions and melt inclusion vapour bubbles commonly contain peaks arising from other gaseous species (e.g., SO<sub>2</sub>, N<sub>2</sub>) or solid phases on the inclusion wall (e.g., carbonates, sulfates, [Schiavi et al. \[2020\]](#), [Frezzotti et al. \[2012\]](#)). It can be helpful to identify which spectra contain such phases, and quantify characteristics of these peaks (e.g., peak heights, positions, relative peak areas, [Burke \[2001\]](#)). As always, step 1 is to obtain all the spectra you wish to fit (Fig. 4). Step 2 uses the function `plot_secondary_peaks` to plot the spectra in a specific wavenumber range from all selected files. Intensities are normalized based on the range of intensities in the selected wavenumber window, allowing multiple spectra to be stacked and inspected. It is clear from this visualization strategy that files #42 and #33 in Step 2 of Fig. 4 have prominent carbonate peaks. For any given set of spectra, you can inspect as many regions as you want. For example, the second panel in Step 2 is centered around the SO<sub>2</sub> peak at  $\sim 1151 \text{ cm}^{-1}$ .

In contrast to just plotting spectra to visually identify secondary phases (`just_plot=True`), the function `plot_secondary_peaks` also identifies peak positions within a user-defined wavenumber range, using either `scipy.find_peaks`, or peaks with a specified deviation above background noise. Identified peaks will be marked on the returned figure with a yellow star (Fig. 4). The function also returns a dataframe of peak parameters (position, height, prominence, and the filename, filled with NaNs when no peaks are found). After identifying spectra containing secondary peaks, peak parameters to fit these peaks are tweaked in Step 3 based on a representative spectra. Using the `model_name` parameter, secondary peaks can be fit with Gaussian, PseudoVoigt or Voigt curves, or a spline. These fit parameters are then applied to all files. More than 1 secondary phase can be identified in a given notebook. In Step 5, all identified secondary peaks are merged together with fitting parameters for diad peaks (see Fig. 3).

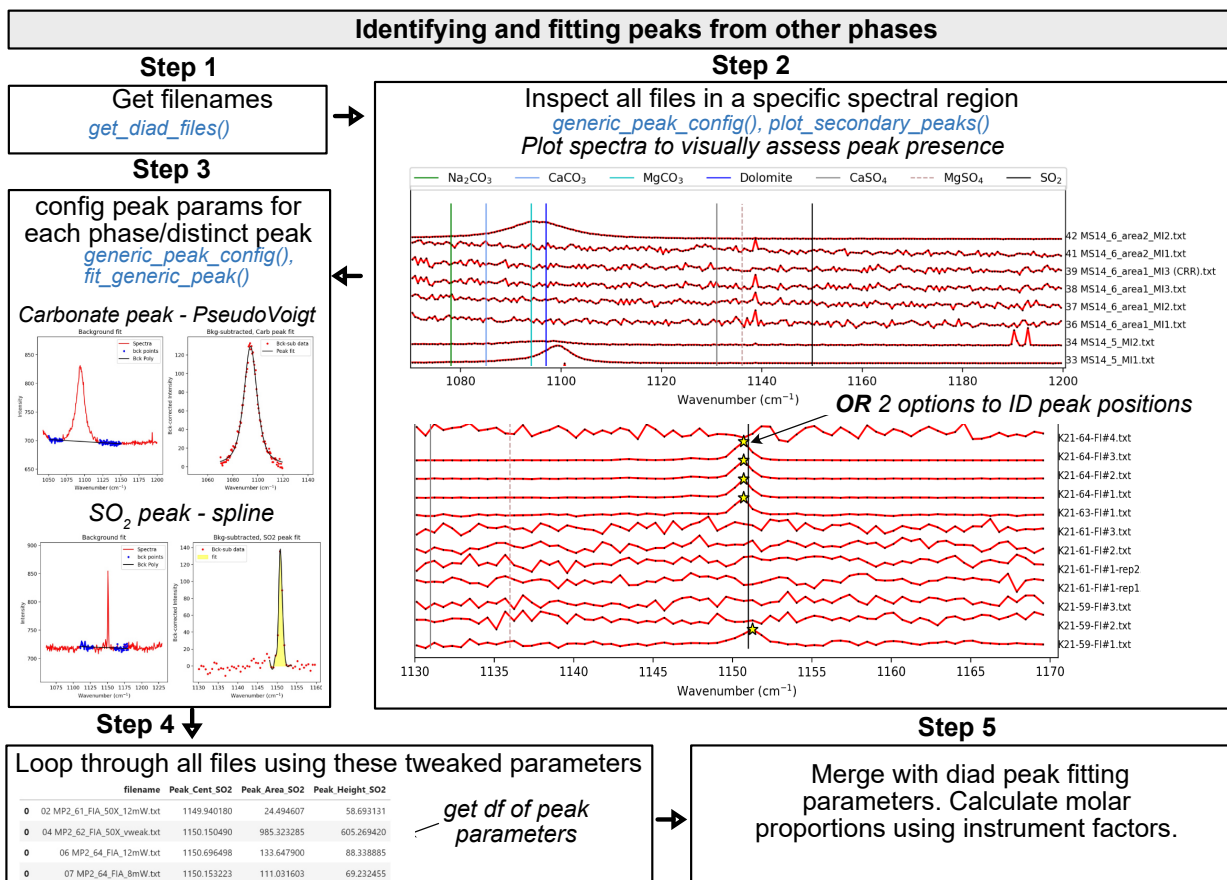


Figure 4: Schematic of workflow used to fit secondary peaks (e.g., carbonate, SO<sub>2</sub>). Multiple secondary peaks can be fitted, and all outputs can be merged with diad fit parameters in Step 5.

## 8 FITTING NE LINES

During any given analytical session, there may be some stretching or contraction of the Raman spectra; these changes are often referred to as 'non-linearity of the Raman shift axis'. For brevity and to draw parallels with various mass spectrometry techniques, we term this 'instrument drift'. We find that these changes often correlate very well with temperature changes in the laboratory. Commonly, instrument drift within the spectral region containing the Fermi diad is assessed by repeatedly measuring the emission spectrum of Neon (Ne) produced by a lamp every  $\sim 5$ -10 minutes. As well as correcting drift during a given session, Ne can also be used to apply a correction factor between sessions, allowing continued use of a Raman densimeter months to years after it was calibrated. On instruments without a Ne lamp, or with insufficient spectral resolution to quantify the narrow Ne peaks, repeated analyses of standard with known CO<sub>2</sub> density may be used instead.

The Ne emission spectrum has a number of distinctive "lines", several of which lie close to the position of the CO<sub>2</sub> Fermi diad. The wavelength of the different Ne lines in air ( $\lambda_1$ ) are converted into Raman shifts ( $\Delta_\nu$ ) in cm<sup>-1</sup> using the excitation wavelength of the laser (e.g.,  $\lambda_0=532.05$  nm; Lin et al. [2007]):

$$\Delta_\nu = \frac{10^7}{\lambda_0(\text{nm})} - \frac{10^7}{\lambda_1(\text{nm})} \quad (4)$$

Traditionally, a given diad acquisition has been corrected for instrument drift and non-linearity by comparing the measured distance between two selected Ne lines ( $\Delta_{\text{Ne}}^{\text{Measured}}$ ) and the theoretical distance between those lines using Equation 4 ( $\Delta_{\text{Ne}}^{\text{Theoretical}}$ ):

$$\text{Correction Factor} = \frac{\Delta_{\text{Ne}}^{\text{Theoretical}}}{\Delta_{\text{Ne}}^{\text{Measured}}} \quad (5)$$

This correction factor is then used to correct the measure diad splitting:

$$\Delta_{\text{CO}_2}^{\text{Corrected}} = \text{Correction Factor} \times \Delta_{\text{CO}_2}^{\text{Measured}} \quad (6)$$

This approach has been termed the 'line segment' technique by Bakker [2021], and a typical workflow of how this method is performed in DiadFit is summarized in Fig. 5. Step 1 identifies all the files which contain Ne lines. Step 2 calculates the theoretical wavenumber of each Ne line using the specific wavelength of your Raman system. You can specify a threshold intensity, and only get lines stronger than that (here, we set the threshold at 2000). This returns a dataframe, with the Raman shift (wavenumber) expected for each Ne line position for your specific wavelength (See Fig. 5 Step 2):

```
df_Ne=pf.calculate_Ne_line_positions(
wavelength=531.885, cut_off_intensity=2000)
```

In Step 3, two Ne lines are selected (1122 cm<sup>-1</sup> and 1453<sup>-1</sup> in this example), and the theoretical splitting is calculated between the closest lines to those specified wavenumbers. In Step 4, one representative file is selected, and used to tweak peak identification parameters, which are then fed into the Scipy `find_peaks` function to identify the approximate position of each Ne line (and its intensity). Obtaining approximate peak positions and intensities greatly improves the computational efficiency of the fitting process. Default peak identification parameters are stored in the data class `Neon_id_config`, such as the height, prominence, width and threshold to use when identifying peaks using SciPy `find_peaks`. The prominence, defined as the vertical distance above the neighbouring background, is the most important parameter to tweak between different instruments (some instruments have peaks 100s-1000s of counts above background while others are 100,000-1 million counts above background). The function `identify_Ne_lines` uses this tweaked configuration file, and identifies the largest peak within  $\pm 10$  datapoints of the Ne line of interest (e.g. for a spectra resolution of 0.4 cm<sup>-1</sup> and for line 1122, the spectral region 1118-1126 cm<sup>-1</sup> would be searched).

After identifying approximate peak positions for each file in Step 4, peak fitting parameters are tweaked in Step 5. The peak fitting function fits a polynomial background to two regions either side of the Ne line, discarding points within this region which are outside of a certain number of standard deviations of the median background position (default  $3\sigma$ , can be tweaked in `Ne_peak_config`). This background is then subtracted. For most Ne lines, a single PseudoVoigt/Voigt curve can be fitted to background-subtracted data (See  $\sim 1447$  cm<sup>-1</sup> peak in Step 6, Fig. 5). For the line at  $\sim 1116$  cm<sup>-1</sup>, two peaks need to be fitted iteratively because of the prominent shoulder to the left of this line (red and cyan curves, combined into the green curve, Fig. 5). Default values specifying how to fit these peaks are stored in a dataclass `Ne_peak_config`, and generally only need tweaking once for each instrument and each selected Ne line. The most important parameters are the positions of the background. These are expressed in terms of distance from the peak center identified above. For example, specifying `lower_bck_pk1=(-40, -25)` positions a background window 40-25 wavenumbers to the left of the peak center. Other important parameters include the degree of polynomial to fit between background points `N_poly_pk1_baseline=2`, and the approximate sigma of the PseudoVoigt/Voigt curve (`pk1_sigma=0.6, pk2_sigma=0.7`). In Step 6, these



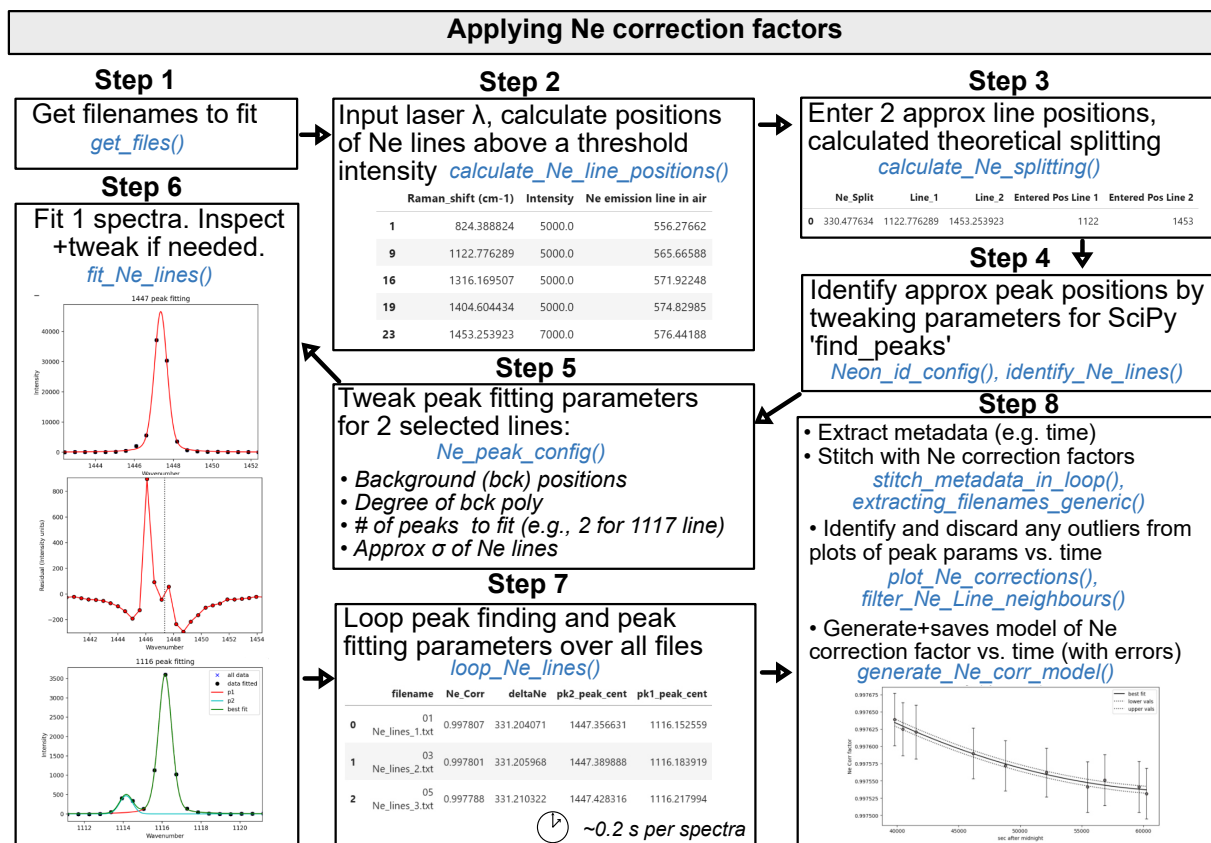


Figure 5: Schematic showing how DiadFit can be used to fit Ne lines, and build a model of correction factor vs. time with full propagation of uncertainty.

tweaked peak fit parameters are used to fit one spectra file with the function `fit_Ne_lines`. This function returns the peak positions and other fit parameters, as well as graphs showing the overall best fit, the residual of the fit, and the background positions. In addition to plots for visual inspection of residuals, the function also calculates a measure of the residual for each peak:

$$Residual = \frac{\sum \sqrt{(y_{meas} - y_{fitted})^2}}{N_{points}} \quad (7)$$

where  $y_{meas}$  is the y-coordinate of the background-subtracted data,  $y_{fitted}$  is the y coordinate of the best composite model fit, and  $N_{points}$  is the number of discrete points along the x axis used in the fit.

After inspecting these graphs for one Neon acquisition and tweaking any fit parameters as necessary (e.g., background positions, plotting parameters), the `Ne_peak_config` file is updated with the sigma values obtained from this example file (rather than the users guess). The tweaked find peaks and peak fit parameters can then be used to loop through all Ne spectra (Step 7). On a regular laptop (e.g., 16 GB RAM, Intel i7), it takes approximately 0.2 s to fit each Ne file. There is also an option for the function to save a figure showing the fit for each file in a subfolder it creates within the spectra path. This increases the run time to 1.2 s for each file, but allows users to check the fits, or publish fits as part of a data repository accompanying a paper. After all files are looped through, DiadFit returns a pandas dataframe with the filename, and all the peak fit parameters (including the all important Ne correction factor).

In most published studies, Fermi diad acquisitions have been corrected using the average correction factor of the Ne line acquired before and after a specific sample (although occasionally concurrent acquisitions are used). However, the relatively narrow shape of the Ne peaks means that the error on the peak center of each line, and thus the Ne correction factor, is relatively large (see error bars on Ne correction factor on Fig. 5). Thus, we suggest it may be better to perform a regression of the correction factor as a function of time to average out this random noise. On many instruments (e.g., WITec, some HORIBAs), the spectral file doesn't include a time stamp. Sometimes (e.g., WITec), the timestamp is stored in the metadata file, meaning that data and metadata files must be stitched together to obtain the time for each Ne correction factor (see documentation for examples). Alternatively, DiadFit contains functions to extract the time based on the read or edit time stamp on the file. Once a DataFrame is obtained that contains both the Ne correction factor and the time (Step 8), it is useful to inspect changes in Neon correction factors and

peak positions with time using built-in visualization functions (e.g., `plot_Ne_corrections`). This allows outliers to be discarded that differ substantially from adjacent acquisitions using the function `filter_Ne_lines_neighbours`. Finally, a polynomial or spline model is used to parameterize the change in Ne correction factor as a function of time (expressed as seconds after midnight, Step 8, Fig. 5), along with the associated confident interval. This model is saved, so that it can be loaded when processing CO<sub>2</sub> spectra from the same session to calculate the correction factor at each point in time (and the associated uncertainty).

### 8.1 A more complex Ne fitting routine

Bakker [2021] criticized the 'line segment' technique, because it assumes that the correction factor at any given point between two lines is the same, which is not true if there is any non-linearity in the spectrometer (Bakker [2021]). It has also been noted that choosing different combinations of Ne lines greatly influences the correction factor (and even the direction of drift within a given analytical session (Wieser et al. [2021])). Bakker [2021] suggest that a model should be developed for how the position of measured Ne lines deviates from the true theoretical position as a function of wavenumber, allowing a correction factor to be applied to each diad position (these corrected diad positions should then be used to calculate splitting). They term this the 'bracketing' technique. Fig. 6a shows the position of Ne lines relative to the Fermi diad from a fluid inclusion collected using a green laser with  $\lambda=532.046$  nm. Fig. 6b shows the deviation of each Ne line from the theoretical position (theoretical/measured position) for 6 different Ne lines over a 24 hour period. For each Ne acquisition, we fit a polynomial through the correction factor for 6 Ne lines to describe the shift as a function of the wavenumber for each discrete acquisition.

These polynomial fits demonstrate that the correction factor is highly non linear across the spectral window of interest. The 'line segment' technique can be visualized by drawing a straight line between any two points on a polynomial curve (Fig. 6c). If the gradient of this linear segment is the same as the gradient of a line drawn between the locations where the diad peaks intercept the polynomial, the line segment technique provides a reasonable approximation of the correction factor. However, it is clear that applying the line segment technique to the 1220-1567 lines (red dashed segment) would result in a Ne correction factor that is far smaller than that determined using the bracketing technique ( $\Delta CF_{brack}=0.9977$  vs.  $\Delta CF_{segment}=0.9991$ ), resulting in a higher apparent diad splitting ( $\Delta CO2_{brack}=103.450$  vs.

---

$\Delta\text{CO}_2_{\text{segment}}=103.648 \text{ cm}^{-1}$ ). In contrast, the line segment method applied to the 1220-1400 lines results in a very similar correction factor to the bracketing technique ( $\Delta\text{CF}_{\text{brack}}=0.9977$  vs.  $\Delta\text{CF}_{\text{segment}}=0.9976$ ). However, the disadvantage of this combination of lines is that the 1220 line is relatively small, resulting in larger fitting errors, meaning that correction factors show substantially more variability in a given run than using the 1117–1447 pair.

While the absolute correction factor clearly varies as a function of the choice of Ne line correction method, in terms of quantifying  $\text{CO}_2$  diads, it is more important to determine how these Ne correction factors change within and between runs. If the offset between the bracketing and line segment techniques is constant, then as long as the relationship between  $\text{CO}_2$  density and diad splitting is calibrated using the same Ne correction technique that is used during instrument measurement, it may not matter. The tedium of fitting Ne lines in existing tools means that no studies have investigated the relative success of different Neon correction routines relative to the instrument specific calibration. DiadFit allows users to easily fit all relevant lines, so non-linearities specific to each individual Raman instrument can be investigated to develop the best Ne correction strategy, and errors associated with different peak fits can be robustly assessed.

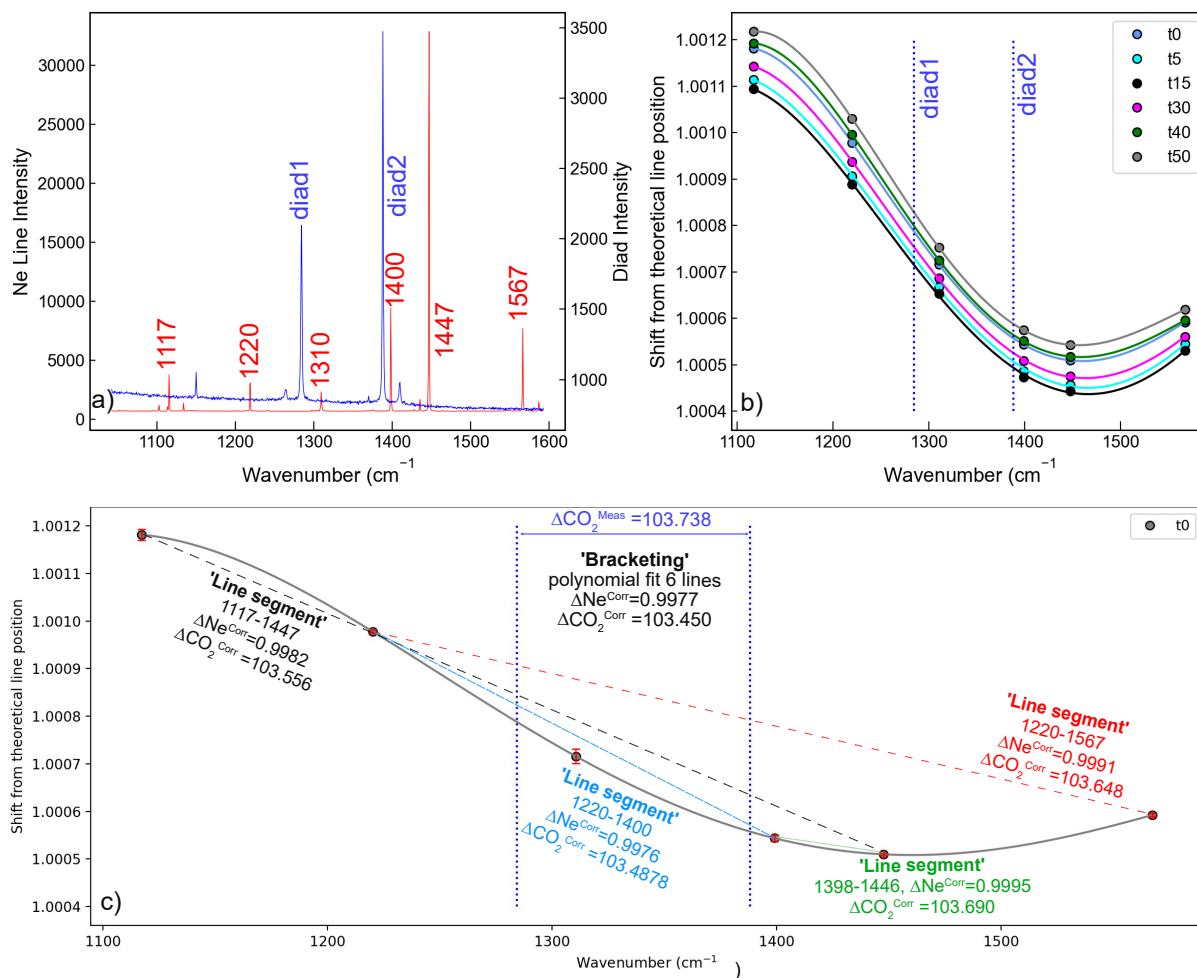


Figure 6: Schematic showing how DiadFit can be used to fit Ne lines, and build a model of correction factor vs. time. Red error bars show that the peak fitting error on the 1117 and 1310 lines are larger than the other peaks (where the error bar is smaller than the symbol size).

## 9 CALCULATIONS INVOLVING THE CO<sub>2</sub> EQUATION OF STATE

An equation of state (EOS) describes the relationship between physical properties of a system such as pressure, temperature and density. DiadFit currently supports calculations using the EOS for pure CO<sub>2</sub> using the model of [Sternner and Pitzer \[1994\]](#) (hereafter SP94) and [Span and Wagner \[1996\]](#) (hereafter SW96). While the SP94 EOS is coded directly into DiadFit, we perform calculations using the SW96 EOS through the Python package CoolProp, requiring installation of this package. There are three core functions used to perform EOS calculations in DiadFit:

1. `calculate_rho_for_P_T`: calculates CO<sub>2</sub> density if P and T are known.
2. `calculate_P_for_rho_T`: calculates P if CO<sub>2</sub> density and T are known.
3. `calculate_T_for_rho_P`: calculates T if P and CO<sub>2</sub> density are known.

In systems in equilibrium with mixed fluids (e.g. H<sub>2</sub>O in arc magmas), the additional complexities of mixed fluids must be accounted for (see [Hansteen and Klugel \[2008\]](#)). Mixed fluid EOS are not currently available in DiadFit, but we hope to add them in future.

### 9.0.1 Calculating CO<sub>2</sub> density for a given P and T

The function `calculate_P_for_rho_T` can be used to calculate CO<sub>2</sub> density for a specified Pressure (P) and Temperature (T). This calculation is very useful when processing data from Raman calibration apparatus, where T is measured by a thermistor, and P is measured with a pressure transducer ([DeVitre et al. \[2021\]](#)). An entire spreadsheet of pressures and temperatures can be imported and all densities calculated:

```
df=pd.read_excel('Cali_Data.xlsx')
dens_SW96=pf.calculate_rho_for_P_T(
P_kbar=df['P_kbar'], T_K=df['T_K'],
EOS='SW96')
```

### 9.1 Calculating pressures from CO<sub>2</sub> densities and temperatures

The function `calculate_P_for_rho_T` can be used to calculate pressure for a specified CO<sub>2</sub> density (rho) and temperature (T). This calculation is commonly used to calculate the entrapment pressure of a fluid inclusion under the assumption that the volume and mass of the inclusion is fixed from the point of entrapment to the point at which it is measured in the lab ([Roedder \[2018\]](#)). For example, to

convert a CO<sub>2</sub> density of 0.5 g/cm<sup>3</sup> into a pressure at a temperature of 1200 K using the [Span and Wagner \[1996\]](#) EOS (SW96):

```
P_SW96=pf.calculate_P_for_rho_T(
CO2_dens_gcm3=0.5, T_K=1200, EOS='SW96')
```

The [Sternner and Pitzer \[1994\]](#) EOS (SP94) can be used instead simply by changing the EOS argument:

```
P_SP94=pf.calculate_P_for_rho_T(
density_gcm3=0.5, T_K=1200, EOS='SW94')
```

This function can also be applied to a pandas dataframe with as many rows as the user wants. For example, we could load an entire spreadsheet with columns for CO<sub>2</sub> densities and an estimate of entrapment temperatures in °C (as well as an optional column with the sample name):

```
df=pd.read_excel('FI_densities.xlsx')
P_SW96=pf.calculate_P_for_rho_T(
T_K=df['Temp in C']+273.15,
CO2_dens_gcm3=df['Density_g_cm3'],
EOS='SW96', Sample_ID=df['Sample'])
```

This returns a pandas dataframe with calculations done for each input row.

	P_kbar	P_MPa	T_K	CO2_dens_gcm3	Sample_ID
0	0.276826	27.682633	1373.15	0.1	FI1
1	1.559737	155.973743	1473.15	0.4	FI2
2	3.789037	378.903651	1423.15	0.7	FI3
3	10.626112	1062.611174	1473.15	1.1	FI4
4	26.062249	2606.224906	1573.15	1.5	FI5

### 9.2 Comparing two EOS

DiadFit makes it very simple to compare calculations using the EOSs of [Sternner and Pitzer \[1994\]](#) and [Span and Wagner \[1996\]](#). In Fig. 7, we calculate pressure for 11 discrete densities between 0.1 and 1.1 g/cm<sup>3</sup> and temperatures between 34 and 2000 °C (worked example given at ReadTheDocs). These calculations would have been extremely tedious in existing tools, but can be performed in several lines of code in DiadFit (and in seconds of computational time). This figure demonstrates that the EOS are extremely similar at the temperatures of basaltic magmas on Earth (<2% discrepancies).

### 9.3 Converting homogenization temperatures to CO<sub>2</sub> densities

Microthermometry provides an alternative method to Raman spectroscopy to determine the density of CO<sub>2</sub>-rich fluids. A fluid inclusion is cooled down,



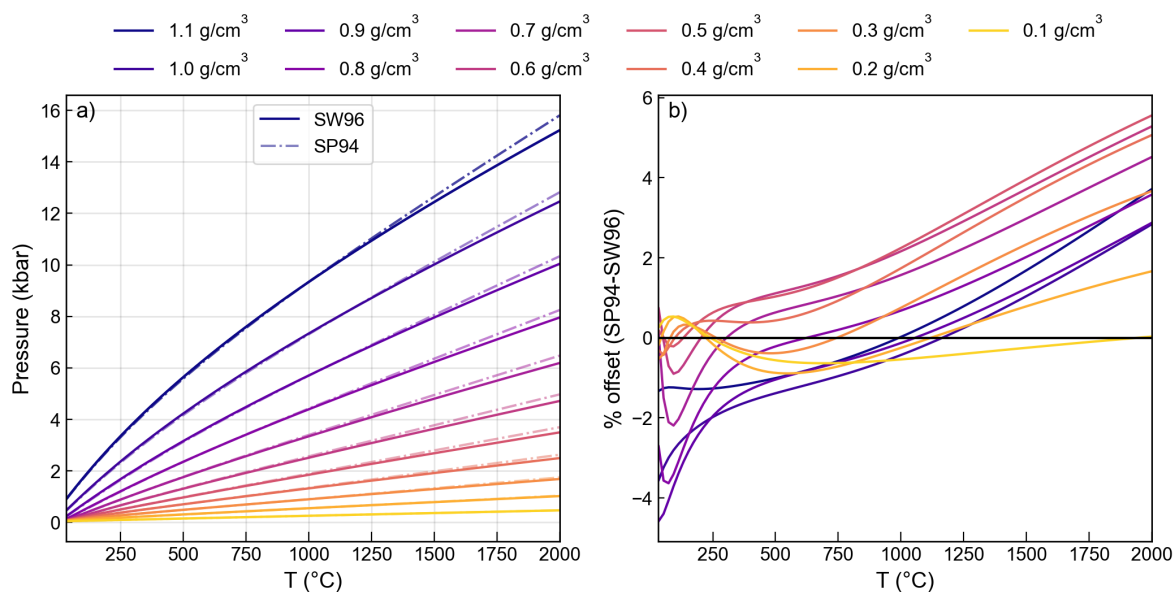


Figure 7: Comparison of the CO<sub>2</sub> EOS of [Sterner and Pitzer \[1994\]](#) and [Span and Wagner \[1996\]](#). The y axis on b) shows the pressure calculated by SP94 minus that from SW96 divided by the average of these two pressures.

and then slowly heated up to determine the temperature at which a mix of liquid and vapour transitions to a single homogenous phase (the homogenization temperature). CO<sub>2</sub> densities can be calculated from these homogenization temperatures using the function `calculate_CO2_density_homog_T`. This function uses the homogenization temperature to calculate the pressure based on the position of the L-V phase boundary from [Span and Wagner \[1996\]](#). Once the pressure is constrained, this is used alongside the homogenization temperature to calculate the CO<sub>2</sub> density using the [Span and Wagner \[1996\]](#) EOS (see [Hansteen \[1991\]](#), [Kobayashi et al. \[2012\]](#)). To calculate the CO<sub>2</sub> density of a fluid inclusion which homogenized at -18 ° to a liquid phase:

```
CalcDens=pf.calculate_CO2_density_homog_T(
T_h_C=-18, homog_to='L')
```

This returns a DataFrame showing the bulk density, the density of the co-existing liquid and vapour at the point of homogenization, and the user-inputted parameters.

	Bulk_gcm3	Liq_gcm3	Gas_gcm3	T_h_C	homog_to
0	1.022329	1.022329	0.055156	-18	L

An entire excel sheet of homogenization temperatures and phases can be loaded as a DataFrame. There is also an optional input of entering a sample name for each row (so it is returned in the outputted DataFrame):

```
pf.calculate_CO2_density_homog_T(
T_h_C=df['T_c_Homog'], SampleID=df['Sample'],
homog_to=df['homog_to'])
```

	Bulk_gcm3	Liq_gcm3	Gas_gcm3	T_h_C	homog_to	Sample_ID
0	0.593263	0.593263	0.345003	30	L	FI1
1	0.710471	0.710471	0.242710	25	L	FI2
2	0.773392	0.773392	0.194204	20	L	FI3
3	0.160735	0.821187	0.160735	15	V	FI4
4	0.861096	0.861096	0.135157	10	L	FI5

Uncertainties in homogenization temperature can be propagated to determine errors in density using Monte-Carlo techniques (see example on [ReadTheDocs](#)).

## 10 ADDITIONAL CALCULATIONS RELATING TO FI BAROMETRY

### 10.1 Converting Pressures into depths

Building on functionality in [Thermobar \(Wieser et al. \[2022\]\)](#), DiadFit can convert entrapment pressures to depths using various options (Fig. 1h) implemented in the function `convert_pressure_to_depth`:

- A fixed crustal density (e.g.,  $\rho=2700 \text{ kg/m}^3$ )
- A 2-step crustal density profile (e.g.,  $\rho=2700 \text{ kg/m}^3$  at <10 km,  $\rho=3300 \text{ kg/m}^3$  at >10 km)
- A 3-step crustal density profile
- Pressure-depth models of:

1. Rasmussen et al. [2022] ('rasmussen')
2. Hill and Zuccal [1987] as parameterized by Putirka [2017] ('hill\_zucca')
3. The combined model of Mavko and Thompson [1983] and DeBari and Greene [2011] as parameterized by Putirka [2017] ('mavko\_debari').
4. Ryan [1988] parameterized by Lerner et al. [2021] ('ryan\_lerner') suitable for use in Hawai'i.

We endeavor to add more profiles relevant to different tectonic settings as they become available.

To calculate depths using the density profile of Lerner et al. [2021] for the pressures calculated using the SW96 EOS above:

```
D_RL=pf.convert_pressure_to_depth(
P_kbar=P_SW96['P_kbar'], mode1='ryan_lerner')
```

This returns a pandas Series of depths in km, which could be appended onto the dataframe produced above:

```
P_SW96['Depth_Ryan_Lerner']=D_RL
```

This function could be used to investigate a number of different pressure-depth conversions, appending each calculated depth onto a single dataframe for easy comparison.

## 11 QUANTIFYING UNCERTAINTY

### 11.1 Uncertainty when determining CO<sub>2</sub> density

DiadFit provides a framework for propagating the three main sources of analytical uncertainty when quantifying CO<sub>2</sub> density by Raman spectroscopy:

1. Error associated with determining the peak center for each CO<sub>2</sub> peak (Fig. 8a-b)
2. Error associated with correcting for instrument drift (Fig. 8a-c)
3. Error associated with the densimeter used to convert drift-corrected splitting into CO<sub>2</sub> density (Fig. 8d)

Diadfit obtains the  $1\sigma$  error associated with each peak center using functionality in lmfit. The error associated with the position of each peak center is combined in quadrature to get the error on the peak splitting. The saved Ne line correction model is used to determine the error for the Ne correction factor (Fig. 8c). This error is combined with the splitting error in quadrature to get the uncertainty in the corrected splitting (black crosses, Fig. 8a). To propagate the uncertainty associated with the densimeter, DiadFit uses the regression model through the gas

calibration data. This error is combined with the error on the corrected splitting to yield the overall error in density (Density g/cm<sup>3</sup>, Fig. 8d). Assessing the relative contribution from each source of uncertainty helps optimization of analytical routines (Fig. 8). If the majority of the error is being introduced at the peak fitting stage, it may be that longer acquisitions are required to get stronger signals, or a higher resolution grating is required. Fig. 8a,f shows that a few acquisitions at  $\sim 0.18\text{--}0.2\text{ g/m}^3$  have far larger peak fitting errors than other acquisitions from the same analytical session. These anomalously large errors would justify inspection of the spectra and fits in more detail, and perhaps re-analysis.

### 11.2 Uncertainty in fluid inclusion pressures

DiadFit can be used to propagate uncertainty when calculating pressures and depths from fluid inclusions based on Raman and microthermometry measurements. The function propagate\_FI\_uncertainty allows users to specify uncertainty in CO<sub>2</sub> density, temperature, and crustal density. For each fluid inclusion, the function generates N duplicates of each input variable following the specified error distribution. Pressure (and depths) are calculated for each of these N duplicates, which these are averaged to obtain the mean, median and standard deviation for each FI. Input errors for each variable can be absolute (e.g.,  $\pm 50\text{ K}$  for temperature) or percentage errors (e.g.,  $\pm 5\%$ ), and can follow a normal or uniform distribution. The function outputs a figure showing the simulation for a single specified fluid inclusion (here, FI1, Fig. 9), in addition to two dataframes. The first dataframe shows the mean, median and standard deviation of calculated pressures and depths for each FI (Fig. 9, Output1). The second dataframe showing the results for all simulations - if N=1000 duplicates and N=10 FIs, the dataframe has 10,000 rows (Fig. 9, Output2).

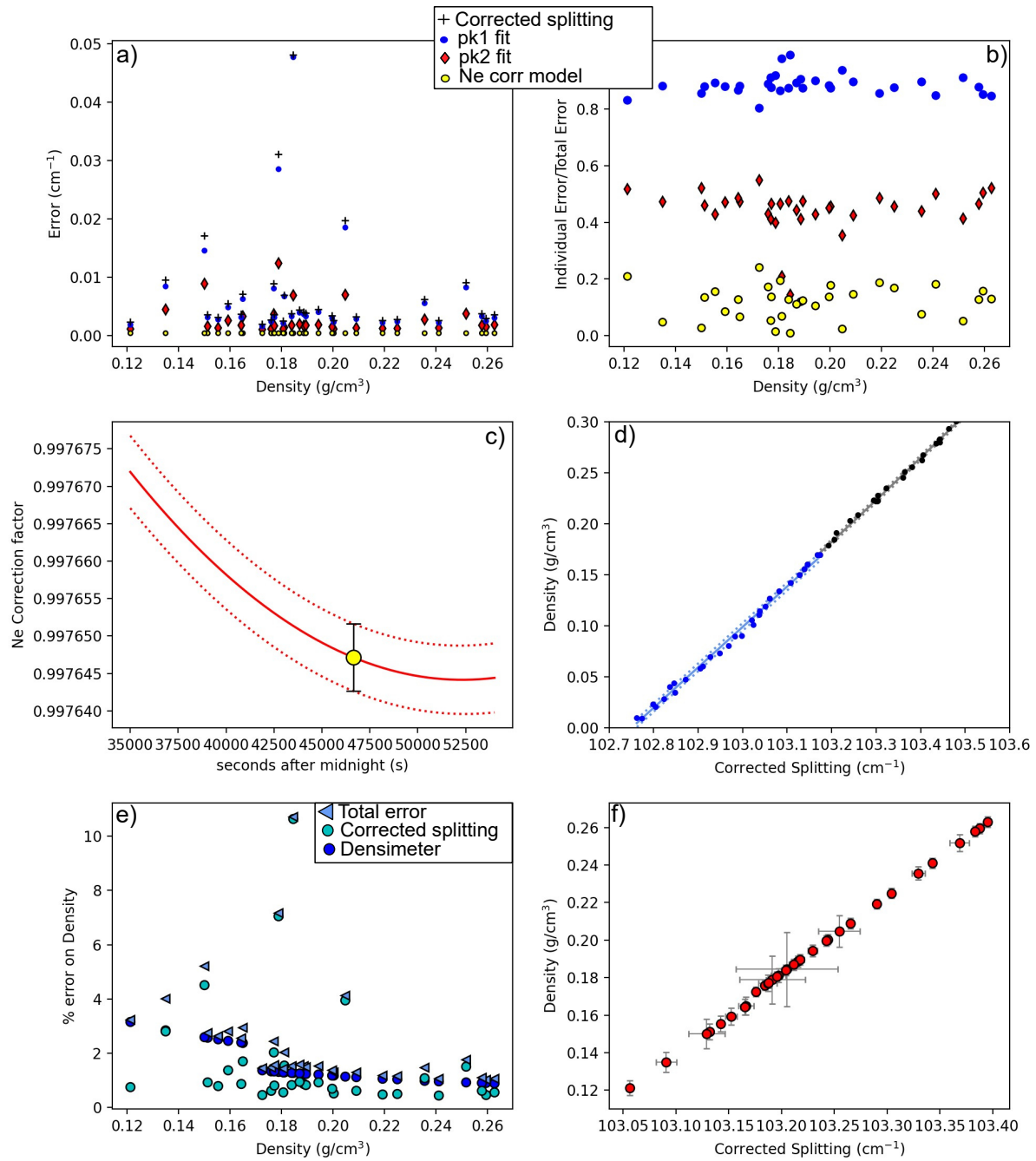


Figure 8: Assessing different sources of analytical error. a) The black cross shows the total error on the corrected splitting from propagating the error in fitting CO<sub>2</sub> peaks and Ne correction model for an instrument with a spectral resolution of 0.56 cm<sup>-1</sup>. Individual contributions from each peak and the Ne correction model are shown. Note, the total error is smaller than the sum of each error shown, as a result of propagating these errors in quadrature. b) To allow easier comparison of the proportional contribution from each source of error, we also take each individual error and divide by the total error on the corrected splitting. This show that the fitting error on pk1 is the largest source of uncertainty. c) Ne regression model with uncertainty represented by red-dashed lines, along with the uncertainty for a single diad acquisition. d) Error associated with the densimeter shown with dashed lines, with the underlying acquisitions shown as dots. The densimeter is regressed in two parts for low and medium densities (see DeVitre et al. [2021]). e) Percentage % error on calculated density, showing the contribution from errors on the corrected splitting (see a) and from the densimeter. f) 1  $\sigma$  errors on density and corrected splitting.

## Propagating uncertainty: CO<sub>2</sub> density to pressure and depth

### Step 1

Load in CO<sub>2</sub> densities ( $\pm$ Temp and other parameters for plotting)

Sample	Density_g_cm3	T_C	Host_Fo_content
F11	0.436888	1048.898738	0.897797
F12	0.417796	1015.924767	0.831850
F14	0.459045	1041.589916	0.883180
F15	0.493865	1034.935183	0.869870

### Step 2

For T, CO<sub>2</sub> and crustal density, select:

- *Magnitude of error, and whether absolute or % (e.g. 5 K, 5%)*
- *Whether error is normally/uniformly distributed*

propagate\_FI\_uncertainty()

### Step 3

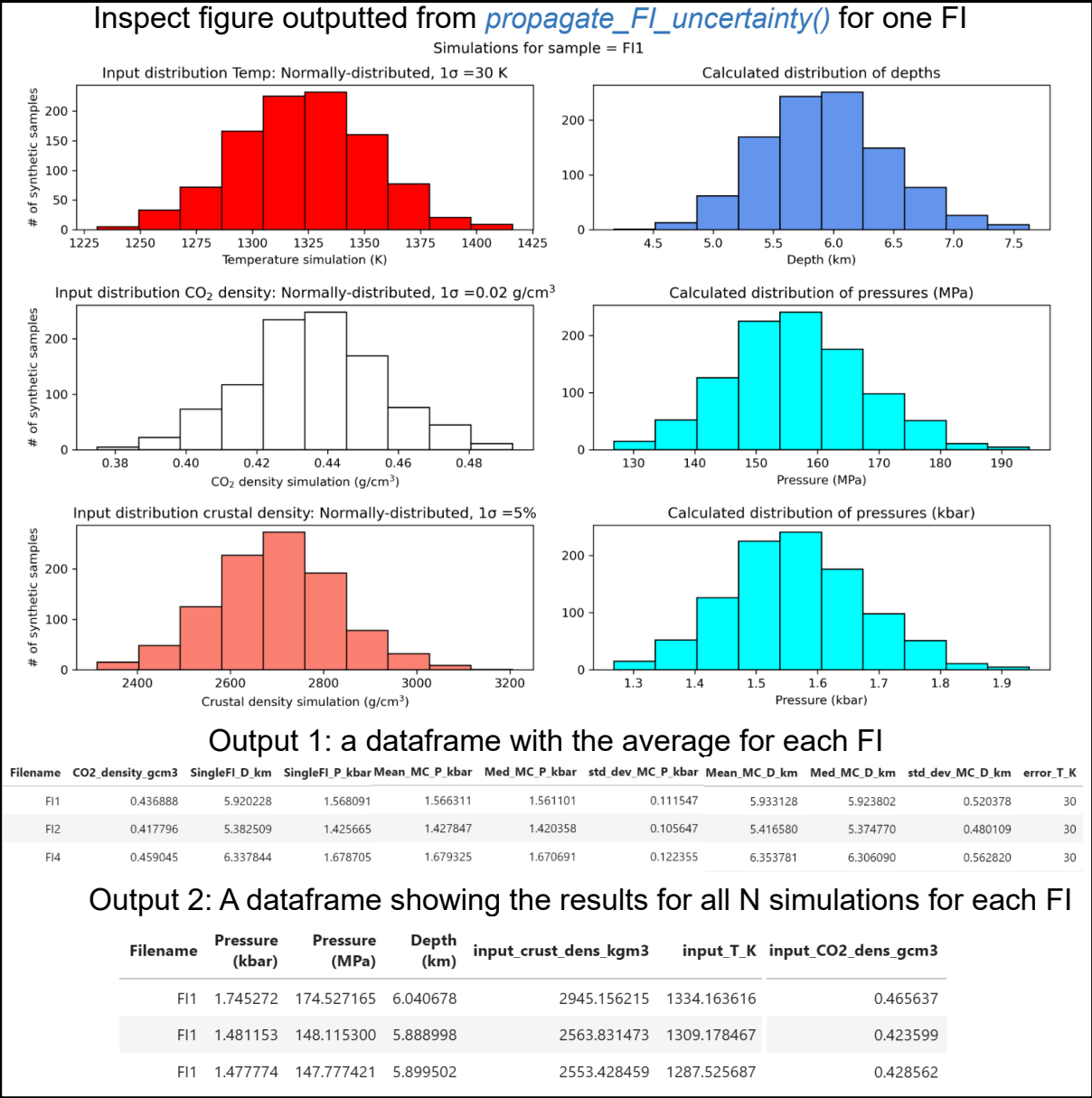


Figure 9: Schematic showing the workflow used to propagate uncertainty in CO<sub>2</sub> density, Temperature, and crustal density into error distributions in pressure and depth for each FI.

### 11.3 Uncertainty in equivalent CO<sub>2</sub> contents of vapour bubbles

The Raman method of reconstructing vapour bubbles present within melt inclusions relies on measuring the CO<sub>2</sub> density, and then converting this into an equivalent amount of CO<sub>2</sub> that would have been dissolved in the glass at the time of melt inclusion entrapment by mass balance:

$$\text{CO}_2^{\text{equivalent glass ppm}} = 10^4 \frac{VB \cdot \text{vol \%} \cdot \rho_{\text{CO}_2}}{\rho_{\text{melt}}} \quad (8)$$

Thus, the uncertainty in the equivalent CO<sub>2</sub> in the glass depends on the error on the CO<sub>2</sub> density measured by Raman spectroscopy, the uncertainty in the bubble volume, and the uncertainty in calculations of the melt density. As for fluid inclusions, DiadFit contains functionality to propagate these uncertainty using Monte-Carlo methods. the function `propagate_CO2_in_bubble` allows users to specify the magnitude of the error for each parameter, whether the error is a % error or an absolute error, and whether the error is normally or uniformly distributed. This function returns two dataframes - the first with the average and standard deviation for each melt inclusion, and the second showing all simulation outputs. This method is particularly powerful when combined with the Python3 tool DensityX which returns the uncertainty on the calculated density [Iacovino and Till \[2019\]](#). Uncertainty on Raman densities can be obtained from DiadFit. Uncertainty in estimating bubble volumes depend greatly on the method used and the geometry of inclusions (e.g., [DeVitre et al. \[2023b\]](#), [Tucker et al. \[2019\]](#)).

## 12 QUANTIFYING PEAK ASYMMETRY TO IDENTIFY CO-EXISTING LIQUID AND GASEOUS CO<sub>2</sub>

At room temperature (18-22 °C), a CO<sub>2</sub> fluid with a density between ~0.18–0.21 and 0.75–0.79 g/cm<sup>3</sup> will consist of an inner shell of CO<sub>2</sub> vapour, and an outer shell of CO<sub>2</sub> liquid ([Span and Wagner \[1996\]](#)). Using the `calculate_CO2_homog_T` function, we can calculate that at 20 °C the gaseous phase will have a density of 0.194 g/cm<sup>3</sup> and the liquid will have a density of 0.773 g/cm<sup>3</sup>. [DeVitre et al. \[2023a\]](#) show that Raman measurements performed in inclusions with two coexisting phases at room temperature don't always show two distinct peaks for the gaseous and liquid CO<sub>2</sub> phase, but often show a single skewed peak, with contributions from both phases. Quantifying peak asymmetry can help to identify such spectra, which cannot be reliably quantified for CO<sub>2</sub> density.

To assess asymmetry in each spectra, an N<sup>th</sup> degree polynomial is fitted between specified baseline positions, and this background is subtracted. A cubic-spline is fitted between the baseline positions, and the x and y coordinate of the highest peak is identified. The position on each shoulder of the peak with an intensity equal to a certain fraction of the peak height is identified. In [Fig. 10](#), this cut off parameter `int_cut_off` is set at 0.3. The ratio of the x-distance between the peak center and these shoulder points (green and grey lines in [Fig. 10](#)) defines the peak asymmetry. After tweaking these parameters for one spectra, the function `loop_diad_skewness` can be used to loop through all files in a specific folder, and stitch the results into a dataframe. Typical skewness parameters have to be identified for each instrument, after which spectra with high skewness can be identified, and re-analysed about the critical temperature where a single peak will be present (see [DeVitre et al. \[2023a\]](#)).

## 13 H<sub>2</sub>O FITTING

Raman spectroscopy can be used to quantify H<sub>2</sub>O within silicate glasses ([Di Genova et al. \[2017\]](#); [Schiavi et al. \[2018\]](#)). There are a number of different methods, with some using the height or intensity of the water Raman band (~3000-3800 cm<sup>-1</sup>), and others using the ratio of the area under the water region divided by the area under the aluminosilicate band at ~200–1250 cm<sup>-1</sup>. Specifically, the glass aluminosilicate region consists of two bands, the low frequency/low wavenumber (LF or LW) band centered on ~550 cm<sup>-1</sup> in [Fig. 11](#), a medium frequency/wavenumber (MF, MW) band centered at ~550 cm<sup>-1</sup>, and a high frequency/wavenumber (HF, HW) band at ~1000 cm<sup>-1</sup>. The exact relationship between peak areas/ratios/heights and the H<sub>2</sub>O content depends on instrument hardware and the glass major element composition, so standards with known H<sub>2</sub>O contents must be used for calibration ([Schiavi et al. \[2018\]](#)).

[Schiavi et al. \[2018\]](#) aim to produce a global calibration, with less dependence on glass composition. They note that the baseline of the silicate region is highly dependent on glass composition and redox state, and suggest fitting a default cubic baseline through predefined baseline positions for 4 melt compositions (basalt, basanite, andesite, rhyolite). They find that the ratio of the total silicate area (LW+HW±MW) to H<sub>2</sub>O area is reasonably independent of melt composition. [González-García et al. \[2021\]](#) note that the presence of nanolites can complicate total silicate area methods, because they produce a peak at 670-690 cm<sup>-1</sup> which can overlap with the LW silicate region used in the 'total area method' of [Schiavi et al. \[2018\]](#). They propose a new protocol using only the HW area to characterize the silicate



## Workflow 3: Peak Asymmetry

### Step 1

Get filenames to fit, select 1 test file

`get_files()`

### Step 2

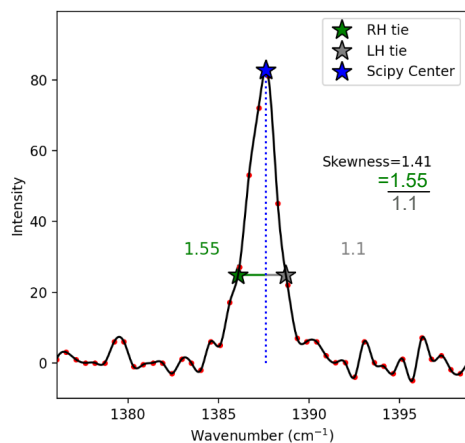
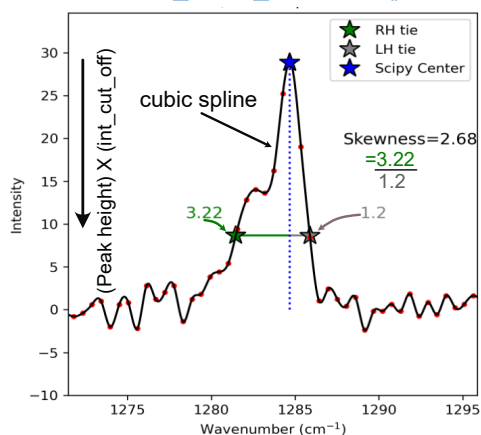
Tweak peak fit parameters+intensity cut off

`diad1_fit_config(), diad2_fit_config()`

### Step 3

Inspect fit to test file, tweak if necessary

`assess_diad1_skewness(),`  
`assess_diad2_skewness()`



### Step 4

Loop through all files using these parameters

`loop_diad_skewness()`

filename	Skewness_diad1	Skewness_diad2
G170_004_1_4_0.5MW_1800G_45S_5ACC (CRR).(1).txt	2.697283	2.037267
G170_004_1_4_0.5MW_1800G_45S_5ACC (CRR).txt	2.681303	1.827020
G170_004_2_4_10MW_1800G_5S_1ACC (CRR).txt	1.075834	1.167500

portion, rather than the the overall silicate region as in [Schiavi et al. \[2020\]](#). DiadFit quantifies the HF, LF and LW areas and the overall silicate area, to allow maximum flexibility when using these different methods (Fig. 11).

When fitting spectra acquired on hydrous glasses in DiadFit, the first step is to select the files of interest. As for diads and Ne lines, we store default peak fit parameters in dataclasses. We have dataclasses for the four suggested background positions of [Schiavi et al. \[2018\]](#), e.g., `sil_bck_pos_Schiavi_basalt`, `sil_bck_pos_Schiavi_andesite`. Users can then tweak these background positions for their specific samples if they wish (e.g. for a basaltic andesite). These dataclasses are also used store the option for baseline fitting. By default, a polynomial of degree 3 is used. For example, the lower background position can be easily changed for basalt from the default of 300–340 to 320–350  $\text{cm}^{-1}$ :


```
pf.sil_bck_pos_Schiavi_basalt(  
lower_range_sil=[320, 350])
```

After subtracting away the background, an  $N^{\text{th}}$  degree polynomial is fitted to the silicate and water regions, and the area under each curve is calculated using the Simpson and the trapezoid method ([Tallarida and Murray \[1987\]](#)) implemented in SciPy and NumPy respectively. The function returns these areas, along with the ratio of the silicate to water areas for each area method (as well as other useful parameters such as the positions of chosen baselines, degrees of polynomials etc. for future reference).

### 13.1 H<sub>2</sub>O fitting within melt inclusions

A common problem when quantifying the amount of CO<sub>2</sub> within vapour bubbles comes from the presence of solid carbonate phases, which sequester carbon. The carbon held within these bubbles isn't accounted for using traditional Raman techniques [Moore et al. \[2015\]](#). [DeVitre et al. \[2023b\]](#) developed a technique where melt inclusions with carbonate-bearing vapour bubbles are heated to their liquidus temperature using a Linkam TS1400XY stage. The main concern regarding any heating method is that it causes diffusive loss of H<sub>2</sub>O from melt inclusions ([Gaetani et al. \[2012\]](#); [Chen et al. \[2011\]](#)) - Raman spectroscopy allows this to be assessed by acquiring spectra before and after heating.

Spectra acquired from melt inclusions which are not exposed is more complicated than quantification of exposed glass, because the Raman signal contains a contribution from the glass and the overlying olivine host. Before fitting the LW-HW silicate fits, the contribution from the host mineral must be subtracted to obtain an 'unmixed spectra', allowing reliable estimation of the silicate area. Here, we

Figure 10: Schematic showing how DiadFit can be  
 Presses universitaires de Strasbourg  
of [DeVitre et al. \[2023a\]](#).

## H<sub>2</sub>O fitting in silicate glasses

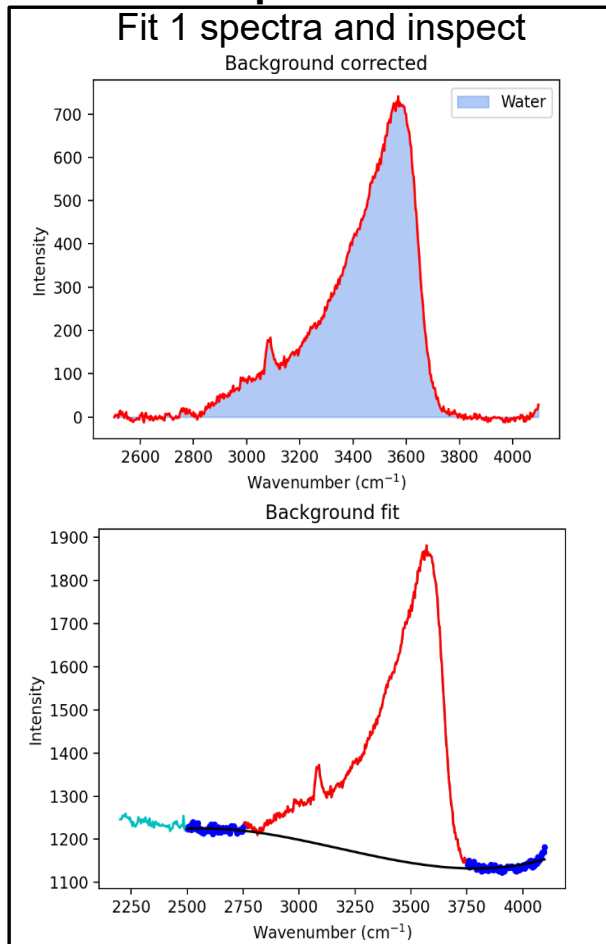
### Step 1

Get filenames of glass spectra  
*get\_files()*

### Step 4

Select peak fit parameters for H<sub>2</sub>O  
*water\_bck\_pos()*

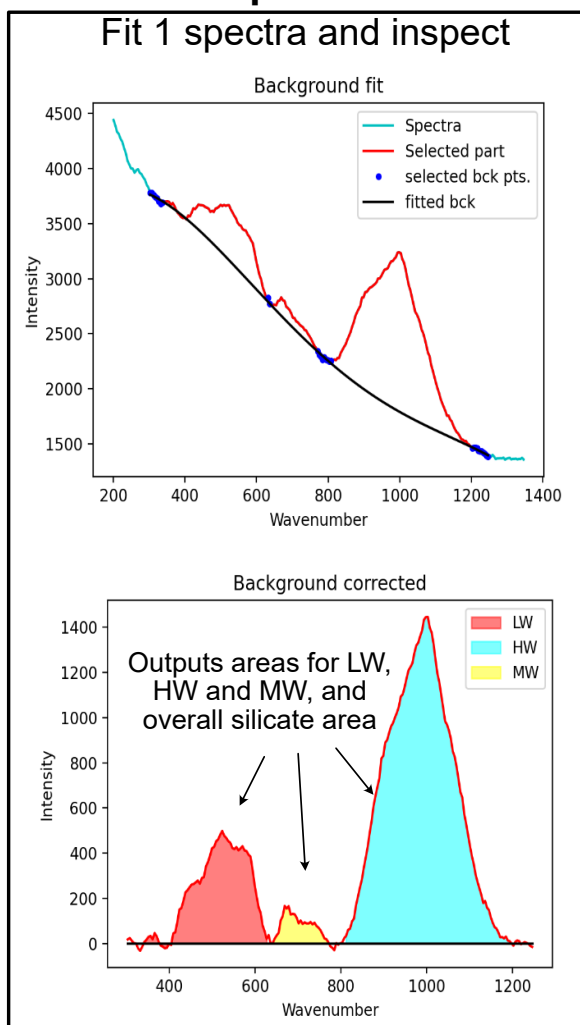
### Step 5



### Step 2

Select peak fit parameters for silicate  
*e.g., sil\_bck\_pos\_Schiavi\_basalt(), sil\_bck\_pos\_Schiavi\_andesite() etc.*

### Step 3



### Step 6

Loop over all files if require similar parameters, or step through and fit 1 at a time, and stitch fits saved in .csvs together

### Step 7

Stitch water and silicate fits together: *stitch\_dataframes\_together()*

MI filename	HW:LW_Trapezoid	HW:LW_Simpson	Water_Trapezoid_Area	MW_Silicate_Trapezoid_Area	MW_Silicate_Simpson_Area
50X_GLASS.txt	0.757968	0.757417	274807.39519	11333.332933	11342.729097

Figure 11: Schematic showing how DiadFit can be used quantify the relative areas of silicate and H<sub>2</sub>O peaks in Raman spectra collected from silicate glasses.

---

describe the method used for olivine-hosted melt inclusions, although it could be easily adapted for other phases. To reliably unmix the spectra, it is best to acquire a spectra in the melt inclusion at the depth where the H<sub>2</sub>O peak is the strongest, and a spectra of the olivine next to the melt inclusions. DiadFit extracts the region of these two spectra between 800-900 cm<sup>-1</sup> containing the strong olivine doublet. A cubic spline is fitted to both spectra to smooth out noise. SciPy is used to find the positions of the two strong peaks in the olivine spectra, and the trough position between these peaks. DiadFit then creates N spectra, where the olivine spectra is subtracted from the mixed spectra. For each of these mixed spectra, a linear regression is fit between the two points with the wavenumbers of the identified olivine peaks. The vertical (y) distance is then calculated between this linear regression and the y value at the x-coordinate of the trough (see Step 4, 12). When too little signal from the olivine has been subtracted from the mixed spectra, the trough position will be lower than the linear regression (e.g., Dist=-400 in sketch 1 on Fig. 12, and when too much olivine has been subtracted, the peaks will invert, and the distance will be a positive number. When exactly the right amount of olivine has been subtracted, there will be no clear peaks or troughs, so the distance will be zero. The function fits a curve to this calculated distance vs. the mixing proportion, to determine the best-fit mixing proportion where the distance is zero. The resulting, "unmixed" spectra is taken as the spectra from the melt inclusion itself. Then, the workflow discussed above can be applied to quantify the relative silicate and H<sub>2</sub>O area.

## H<sub>2</sub>O fitting in olivine-hosted melt inclusions (MIs)

### Step 1

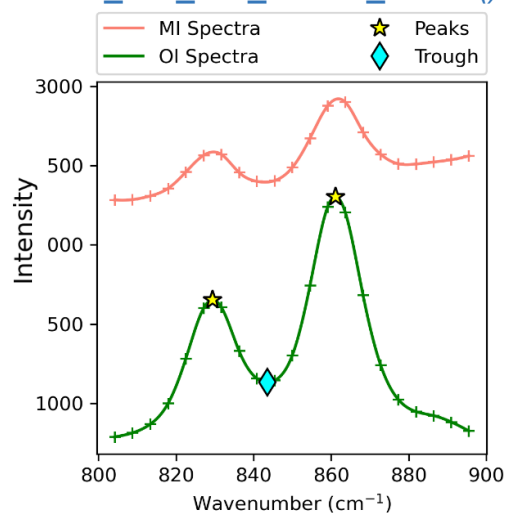
Get filenames of spectra from MIs and neighbouring Ol crystals

*get\_files()*

### Step 3

Extra region around ~800-900 cm<sup>-1</sup> for both spectra. Fit a smoothed cubic spline + ID peaks and troughs

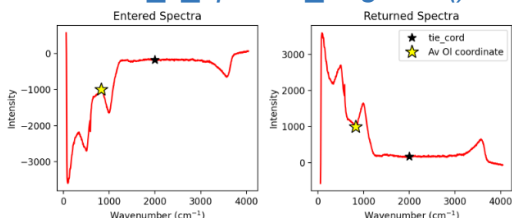
*get\_spectra(),  
smooth\_and\_trim\_around\_olivine()*



### Step 5

Check if unmixed spectra inverted (using 2 tiepoints). Flip if so

*check\_if\_spectra\_negative()*



### Step 6+ = See Fig. 11 - 'H<sub>2</sub>O fitting in silicate glasses'

### Step 2

Find common parts of file name (e.g., xstal, MI name) to pair up MI+Ol files. Select 1 pair.

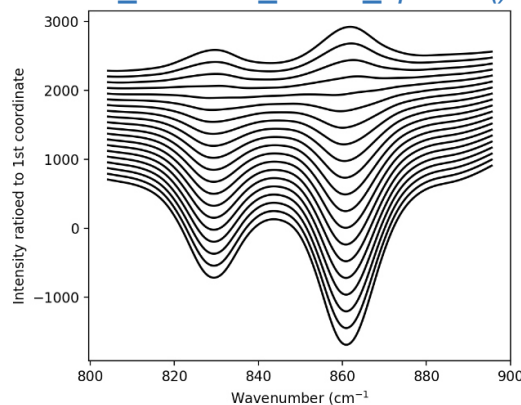
*extract\_xstal\_MI\_name()*

filename_x	crystal_name	MI_name	filename_y
02 CC14_MI2_H2O_96mw.txt	CC14	MI2	03 CC14_MI2_OL_96mw.txt
05 CC13_MI4_H2O.txt	CC13	MI4	06 CC13_MI4_OL.txt

### Step 4

Subtract varying proportions of Ol from the MI spectra.

*make\_evaluate\_mixed\_spectra()*



Best match when y distance between 2 peaks and trough is as small as possible in unmixed spectra

MI-0.1\* Ol

MI-0.9\* Ol

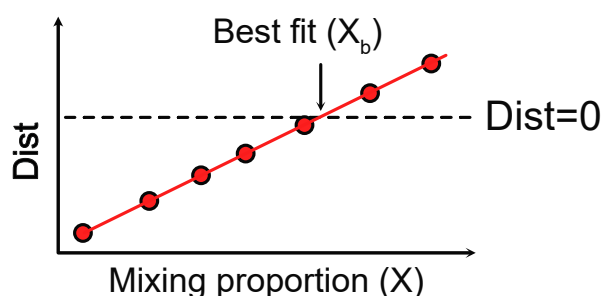
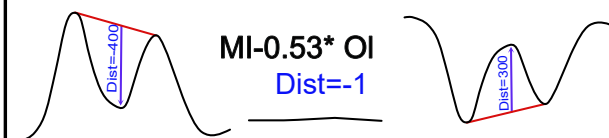


Figure 12: Schematic showing how DiadFit can be used to unmix the contribution of olivine and glass from spectra taken on unexposed melt inclusions. The code could be easily adapted for other silicate phases. There is an option to loop if glass compositions are sufficiently similar. Alternatively, each file can be stepped through manually to tweak positions, and the code saves the output for each file to a .csv, and these are then stitched together after all files are fitted.

## 14 FUTURE WORK

The open-source nature of DiadFit means that users can customize functions and build their own (either on a local fork, or using a pull request on GitHub). Additionally, we anticipate that we will continue to add workflows as new applications of Raman spectroscopy appear in volcanology. To reflect the evolving nature of this tool, when citing DiadFit, users should make sure they specify the version they used, obtained using:

```
pf.__version__
```

Care should also be taken to cite the root packages used by DiadFit. E.g., if converting CO<sub>2</sub> densities to pressures using the functions here, we recommend wording similar to this: "CO<sub>2</sub> densities were converted into pressures using DiadFit (Wieser and DeVitre, 2023, v.1.0), using the Equation of State of Span and Wagner [1996] implemented in CoolProp (Bell et al. [2014]).

## 15 CONCLUSIONS

DiadFit will greatly reduce the time required to fit Raman spectral data for volcanological applications, as well as increasing reproducibility between studies. The robust handling of errors and ability to propagate uncertainty using Monte-Carlo methods allows a better grasp of the errors associated with melt and fluid inclusion workflows. DiadFit also simplifies many workflows involving CO<sub>2</sub> equation of state calculations, for many scientific que Less time peak fitting = more time for science!

## ACKNOWLEDGEMENTS

We are grateful to Felix Boschetty, Lowell Moore, Chelsea Allison, Sarah Hickernell, and Kenneth Befus for providing example Raman file formats from different instruments. We thank Lyndsey Fisher, and Kyle Dayton for providing feedback on the code. PW and CD was supported by UC Berkeley start up funds, the Rose Hills innovator award and NSF grant 2217371.

## AUTHOR CONTRIBUTIONS

PW conceived the project, and wrote the majority of the code, with discussions with CD of how best to implement various procedures. CD wrote the cosmic ray removal code and the code to calculate molar proportions from gas peak areas, and came up with the idea for the peak asymmetry method. She performed extensive testing and tweaking of existing functions.

## DATA AVAILABILITY

All files are available on GitHub <https://github.com/PennyWieser/DiadFit>. Documentation is available at ReadTheDocs ([bit.ly/DiadFitRTD](https://bit.ly/DiadFitRTD)), and YouTube videos explaining various aspects of the tool are available on the DiadFit YouTube channel [bit.ly/DiadFitYouTube](https://bit.ly/DiadFitYouTube).

## REFERENCES

- Allison, C. M., Roggensack, K., and Clarke, A. B. (2021). Highly explosive basaltic eruptions driven by co<sub>2</sub> exsolution. *Nature communications*, 12(1):1–10.
- Bakker, R. J. (2021). The perfection of raman spectroscopic gas densimeters. *Journal of Raman Spectroscopy*, 52(11):1923–1948.
- Bell, I. H., Wronski, J., Quoilin, S., and Lemort, V. (2014). Pure and pseudo-pure fluid thermophysical property evaluation and the open-source thermophysical property library coolprop. *Industrial & engineering chemistry research*, 53(6):2498–2508.
- Burke, E. A. (2001). Raman microspectrometry of fluid inclusions. *Lithos*, 55(1-4):139–158.
- Chen, Y., Provost, A., Schiano, P., and Cluzel, N. (2011). The rate of water loss from olivine-hosted melt inclusions. *Contributions to Mineralogy and Petrology*, 162:625–636.
- Dayton, K., Gazel, E., Wieser, P., Troll, V. R., Carracedo, J. C., La Madrid, H., Roman, D. C., Ward, J., Aulinas, M., Geiger, H., et al. (2023). Deep magma storage during the 2021 la palma eruption. *Science Advances*, 9(6):eade7641.
- DeBari, S. M. and Greene, A. R. (2011). Vertical stratification of composition, density, and inferred magmatic processes in exposed arc crustal sections. In *Arc-continent collision*, pages 121–144. Springer.
- DeVitre, C., Dayton, K., Gazel, E., Pamukcu, A., Gaetani, G., and Wieser, P. (2023a). Laser heating effect on raman analysis of co<sub>2</sub> co-existing as liquid and vapor in olivine-hosted melt inclusion bubbles. *Volcanica*.
- DeVitre, C. L., Allison, C. M., and Gazel, E. (2021). A high-precision co<sub>2</sub> densimeter for raman spectroscopy using a fluid density calibration apparatus. *Chemical Geology*, 584:120522.
- DeVitre, C. L., Gazel, E., Ramalho, R. S., Venugopal, S., Steele-MacInnis, M., Hua, J., Allison, C. M., Moore, L. R., Carracedo, J. C., and Monteleone, B. (2023b). Oceanic intraplate explosive eruptions fed directly from the mantle.



- Proceedings of the National Academy of Sciences*, 120(33):e2302093120.
- Di Genova, D., Sicola, S., Romano, C., Vona, A., Fanara, S., and Spina, L. (2017). Effect of iron and nanolites on raman spectra of volcanic glasses: A reassessment of existing strategies to estimate the water content. *Chemical Geology*, 475:76–86.
- Fermi, E. (1931). Über den ramaneffekt des kohlendioxyds. *Zeitschrift für Physik*, 71:250–259.
- Frezzotti, M. L., Tecce, F., and Casagli, A. (2012). Raman spectroscopy for fluid inclusion analysis. *Journal of Geochemical Exploration*, 112:1–20.
- Fukura, S., Mizukami, T., Odake, S., and Kagi, H. (2006). Factors determining the stability, resolution, and precision of a conventional raman spectrometer. *Applied Spectroscopy*, 60(8):946–950.
- Gaetani, G. A., O’Leary, J. A., Shimizu, N., Bucholz, C. E., and Newville, M. (2012). Rapid reequilibration of h<sub>2</sub>o and oxygen fugacity in olivine-hosted melt inclusions. *Geology*, 40(10):915–918.
- Giordano, D., Russell, J. K., González-García, D., Bersani, D., Dingwell, D. B., and Del Negro, C. (2020). Raman spectroscopy from laboratory and proximal to remote sensing: a tool for the volcanological sciences. *Remote Sensing*, 12(5):805.
- González-García, D., Giordano, D., Allabar, A., Andrade, F., Polo, L., Janasi, V. d. A., Lucchetti, A., Hess, K.-U., De Campos, C., and Dingwell, D. (2021). Retrieving dissolved h<sub>2</sub>o content from micro-raman spectroscopy on nanolitized silicic glasses: application to volcanic products of the paraná magmatic province, brazil. *Chemical Geology*, 567:120058.
- González-García, D., Giordano, D., Russell, J. K., and Dingwell, D. B. (2020). A raman spectroscopic tool to estimate chemical composition of natural volcanic glasses. *Chemical Geology*, 556:119819.
- Hansteen, T. H. (1991). Multi-stage evolution of the picritic maelifell rocks, sw iceland: constraints from mineralogy and inclusions of glass and fluid in olivine. *Contributions to Mineralogy and Petrology*, 109(2):225–239.
- Hansteen, T. H. and Klugel, A. (2008). Fluid inclusion thermobarometry as a tracer for magmatic processes. *Reviews in Mineralogy and Geochemistry*, 69(1):143–177.
- Harris, C. R., Millman, K. J., van der Walt, S. J., Gommers, R., Virtanen, P., Cournapeau, D., Wieser, E., Taylor, J., Berg, S., Smith, N. J., et al. (2020). Array programming with numpy. *Nature*, 585(7825):357–362.
- Hartley, M. E., Maclennan, J., Edmonds, M., and Thordarson, T. (2014). Reconstructing the deep co<sub>2</sub> degassing behaviour of large basaltic fissure eruptions. *Earth and Planetary Science Letters*, 393:120–131.
- Hill, D. P. and Zuccal, J. J. (1987). Geophysical constraints on the structure of. *US Geological Survey Professional Paper*, 2(1350):903.
- Hunter, J. D. (2007). Matplotlib: A 2d graphics environment. *Computing in Science & Engineering*, 9(3):90–95.
- Iacovino, K. and Till, C. B. (2019). Densityx: A program for calculating the densities of magmatic liquids up to 1,627 c and 30 kbar. *Volcanica*, 2(1):1–10.
- Kobayashi, T., Yamamoto, J., Hirajima, T., Ishibashi, H., Hirano, N., Lai, Y., Prikhod’Ko, V. S., and Arai, S. (2012). Conformity and precision of co<sub>2</sub> densimetry in co<sub>2</sub> inclusions: Microthermometry versus raman microspectroscopic densimetry. *Journal of Raman Spectroscopy*, 43(8):1126–1133.
- Lamadrid, H., Moore, L., Moncada, D., Rimstidt, J., Burruss, R., and Bodnar, R. (2017). Reassessment of the raman co<sub>2</sub> densimeter. *Chemical Geology*, 450:210–222.
- Lerner, A. H., Wallace, P. J., Shea, T., Mourey, A. J., Kelly, P. J., Nadeau, P. A., Elias, T., Kern, C., Clor, L. E., Gansecki, C., et al. (2021). The petrologic and degassing behavior of sulfur and other magmatic volatiles from the 2018 eruption of kīlauea, hawaii: melt concentrations, magma storage depths, and magma recycling. *Bulletin of Volcanology*, 83(6):1–32.
- Lin, F., Bodnar, R., and Becker, S. (2007). Experimental determination of the raman ch<sub>4</sub> symmetric stretching ( $\nu_1$ ) band position from 1–650 bar and 0.3–22 c: Application to fluid inclusion studies. *Geochimica et Cosmochimica Acta*, 71(15):3746–3756.
- Mavko, B. B. and Thompson, G. A. (1983). Crustal and upper mantle structure of the northern and central sierra nevada. *Journal of Geophysical Research: Solid Earth*, 88(B7):5874–5892.
- Moore, L. R., Gazel, E., Tuohy, R., Lloyd, A. S., Esposito, R., Steele-MacInnis, M., Hauri, E. H., Wallace, P. J., Plank, T., and Bodnar, R. J. (2015). Bubbles matter: An assessment of the contribution of vapor bubbles to melt inclusion volatile budgets. *American Mineralogist*, 100(4):806–823.
- Morizet, Y., Brooker, R. A., Iacono-Marziano, G., and Kjarsgaard, B. A. (2013). Quantification of dissolved co<sub>2</sub> in silicate glasses using



- micro-raman spectroscopy. *American Mineralogist*, 98(10):1788–1802.
- Newville, M., Stensitzki, T., Allen, D. B., Rawlik, M., Ingargiola, A., and Nelson, A. (2016). Lmfit: Non-linear least-square minimization and curve-fitting for python. *Astrophysics Source Code Library*, pages ascl–1606.
- pandas development team, T. (2020). pandas-dev/pandas: Pandas.
- Putirka, K. D. (2017). Down the crater: where magmas are stored and why they erupt. *Elements*, 13(1):11–16.
- Rasmussen, D. J., Plank, T. A., Roman, D. C., and Zimmer, M. M. (2022). Magmatic water content controls the pre-eruptive depth of arc magmas. *Science*, 375(6585):1169–1172.
- Roedder, E. (2018). Reviews in mineralogy. In *Fluid inclusions*, pages II–II. De Gruyter.
- Rosso, K. and Bodnar, R. (1995). Microthermometric and raman spectroscopic detection limits of CO<sub>2</sub> in fluid inclusions and the raman spectroscopic characterization of CO<sub>2</sub>. *Geochimica et Cosmochimica Acta*, 59(19):3961–3975.
- Ryan, M. P. (1988). The mechanics and three-dimensional internal structure of active magmatic systems: Kilauea volcano, hawaii. *Journal of Geophysical Research: Solid Earth*, 93(B5):4213–4248.
- Schiavi, F., Bolfan-Casanova, N., Buso, R., Laumonier, M., Laporte, D., Medjoubi, K., Venugopal, S., Gómez-Ulla, A., Cluzel, N., and Hardiagon, M. (2020). Quantifying magmatic volatiles by raman microtomography of glass inclusion-hosted bubbles. *Geochemical Perspectives Letters*, 16:17–24.
- Schiavi, F., Bolfan-Casanova, N., Withers, A. C., Médard, E., Laumonier, M., Laporte, D., Flaherty, T., and Gómez-Ulla, A. (2018). Water quantification in silicate glasses by raman spectroscopy: Correcting for the effects of confocality, density and ferric iron. *Chemical Geology*, 483:312–331.
- Span, R. and Wagner, W. (1996). A new equation of state for carbon dioxide covering the fluid region from the triple-point temperature to 1100 K at pressures up to 800 mpa. *Journal of physical and chemical reference data*, 25(6):1509–1596.
- Steele-Macinnis, M., Esposito, R., and Bodnar, R. J. (2011). Thermodynamic model for the effect of post-entrapment crystallization on the H<sub>2</sub>O–CO<sub>2</sub> systematics of vapor-saturated, silicate melt inclusions. *Journal of Petrology*, 52(12):2461–2482.
- Sterner, S. M. and Pitzer, K. S. (1994). An equation of state for carbon dioxide valid from zero to extreme pressures. *Contributions to Mineralogy and Petrology*, 117(4):362–374.
- Tallarida, R. J. and Murray, R. B. (1987). Area under a curve: trapezoidal and simpson's rules. In *Manual of Pharmacologic Calculations*, pages 77–81. Springer.
- Tucker, J. M., Hauri, E. H., Pietruszka, A. J., Garcia, M. O., Marske, J. P., and Trusdell, F. A. (2019). A high carbon content of the hawaiian mantle from olivine-hosted melt inclusions. *Geochimica et Cosmochimica Acta*, 254:156–172.
- Virtanen, P., Gommers, R., Oliphant, T. E., Haberland, M., Reddy, T., Cournapeau, D., Burovski, E., Peterson, P., Weckesser, W., Bright, J., van der Walt, S. J., Brett, M., Wilson, J., Millman, K. J., Mayorov, N., Nelson, A. R. J., Jones, E., Kern, R., Larson, E., Carey, C. J., Polat, İ., Feng, Y., Moore, E. W., VanderPlas, J., Laxalde, D., Perktold, J., Cimrman, R., Henriksen, I., Quintero, E. A., Harris, C. R., Archibald, A. M., Ribeiro, A. H., Pedregosa, F., van Mulbregt, P., and SciPy 1.0 Contributors (2020). SciPy 1.0: Fundamental Algorithms for Scientific Computing in Python. *Nature Methods*, 17:261–272.
- Wang, W. and Lu, W. (2022). High-precision carbon isotopic composition estimation for individual CO<sub>2</sub> fluid inclusions through raman spectroscopy. *Geoscience Frontiers*, page 101528.
- Wang, X., Chou, I.-M., Hu, W., Burruss, R. C., Sun, Q., and Song, Y. (2011). Raman spectroscopic measurements of CO<sub>2</sub> density: Experimental calibration with high-pressure optical cell (hPOC) and fused silica capillary capsule (fSCC) with application to fluid inclusion observations. *Geochimica et Cosmochimica Acta*, 75(14):4080–4093.
- Wieser, P., Petrelli, M., Lubbers, J., Wieser, E., Ozaydin, S., Kent, A., and Till, C. (2022). Thermobar: an open-source python3 tool for thermobarometry and hygrometry. *Volcanica*, 5(2):349–384.
- Wieser, P. E., Lamadrid, H., MacLennan, J., Edmonds, M., Matthews, S., Iacovino, K., Jenner, F. E., Gansecki, C., Trusdell, F., Lee, R. L., et al. (2021). Reconstructing magma storage depths for the 2018 kilauean eruption from melt inclusion CO<sub>2</sub> contents: the importance of vapor bubbles. *Geochemistry, Geophysics, Geosystems*, 22(2):e2020GC009364.
- Wojdyr, M. (2010). Fityk: a general-purpose peak fitting program. *Journal of Applied Crystallography*, 43(5-1):1126–1128.

Yuan, X. and Mayanovic, R. A. (2017). An empirical study on raman peak fitting and its application to raman quantitative research. *Applied spectroscopy*, 71(10):2325–2338.